HHS Public Access

Author manuscript

Nat Immunol. Author manuscript; available in PMC 2020 August 04.

Published in final edited form as:

Nat Immunol. 2020 May ; 21(5): 535–545. doi:10.1038/s41590-020-0663-z.

Adaptive response to inflammation contributes to sustained myelopoiesis and confers a competitive advantage in myelodysplastic syndrome HSCs

Tomoya Muto[1], **Callum S. Walker**[1], **Kwangmin Choi**[1], **Kathleen Hueneman**[1], **Molly A. Smith**[1], **Zartash Gul**[2], **Guillermo Garica-Manero**[3], **Averil Ma**[4], **Yi Zheng**[1,5], **Daniel T. Statczynowski**[1,5,6,✉]

[1]Division of Experimental Hematology and Cancer Biology, Cincinnati Children's Hospital Medical Center, Cincinnati, OH, USA

[2]Department of Internal Medicine, University of Cincinnati, Cincinnati, OH, USA

[3]Department of Leukemia, The University of Texas MD Anderson Cancer Center, Houston, TX, USA

[4]Department of Medicine, University of California, San Francisco, San Francisco, CA, USA

[5]Department of Pediatrics, Cincinnati Children's Hospital Medical Center, Cincinnati, OH, USA

[6]Department of Cancer Biology, University of Cincinnati, Cincinnati, OH, USA

Abstract

Despite evidence of chronic inflammation in myelodysplastic syndrome (MDS) and cell-intrinsic dysregulation of Toll-like receptor (TLR) signaling in MDS hematopoietic stem and progenitor cells (HSPCs), the mechanisms responsible for the competitive advantage of MDS HSPCs in an inflammatory milieu over normal HSPCs remain poorly defined. Here, we found that chronic inflammation was a determinant for the competitive advantage of MDS HSPCs and for disease

✉**Correspondence and requests for materials** should be addressed to D.T.S. Daniel.Starczynowski@cchmc.org.

Author contributions

T.M. and D.T.S. contributed to study conception and design. T.M., C.S.W., K.C., K.H. and M.S. acquired, analyzed and interpreted data. Z.G. and G.G.-M. provided samples. A.M. and Y.Z. provided reagents. T.M. and D.T.S. wrote and revised the manuscript.

Competing interests

D.T.S. serves on the scientific advisory board at Kurome Therapeutics. All other authors declare no competing interests.

Online content

Any methods, additional references, Nature Research reporting summaries, source data, extended data, supplementary information, acknowledgements, peer review information; details of author contributions and competing interests; and statements of data and code availability are available at https://doi.org/10.1038/s41590020-0663-z.

Data availability

The data that support the findings of this study are available from the corresponding author upon request. All gene expression data are available at GSE142560, GSE19429, GSE58831 and GSE88949. Source data for Figs. 2–7 and Extended Data Figs. 1,3, 5 and 8 are presented with the paper.

Additional information

Extended data is available for this paper at https://doi.org/10.1038/s41590-020-0663-z.

Supplementary information is available for this paper at https://doi.org/10.1038/s41590-020-0663-z.

Peer review information Ioana Visan was the primary editor on this article and managed its editorial process and peer review in collaboration with the rest of the editorial team.

progression. The cell-intrinsic response of MDS HSPCs, which involves signaling through the noncanonical NF-kB pathway, protected these cells from chronic inflammation as compared to normal HSPCs. In response to inflammation, MDS HSPCs switched from canonical to noncanonical NF-kB signaling, a process that was dependent on TLR-TRAF6-mediated activation of A20. The competitive advantage of TLR-TRAF6-primed HSPCs could be restored by deletion of A20 or inhibition of the noncanonical NF-kB pathway. These findings uncover the mechanistic basis for the clonal dominance of MDS HSPCs and indicate that interfering with noncanonical NF-kB signaling could prevent MDS progression.

MDS arises from a mutant hematopoietic stem cell (HSC) and is defined by myeloid cell dysplasia and ineffective hematopoiesis[1]. The competitive advantage of clonally derived HSPCs in MDS is supported by genetic analyses of purified HSPCs, which has indicated that most HSCs and myeloid progenitors in MDS patients harbor cytogenetic alterations or mutations[2,3]. The expansion of the myeloid-biased HSPCs seen in humans is also observed in select murine models of MDS[4,5]. These studies indicate that MDS HSPCs acquire increased self-renewal and myeloid progenitor function, which may account for the clonal dominance and for disease progression. However, MDS HSPCs have defects in multi-lineage differentiation, grow inefficiently ex vivo and show poor engraftment in immune-compromised mice[2,6]. Moreover, most of the molecular alterations observed in MDS are not sufficient to explain the increase in the self-renewal potential of MDS HSPCs. Thus, understanding the discrepancy between the clonal dominance of MDS HSPCs and their functional impairment is required to improve treatment of MDS.

One possibility is that alterations in the expression of microenvironmental factors could favor the expansion of MDS HSPCs. A variation of this thesis would posit that microenvironmental factors in MDS would not be conducive for the function of normal HSPC, while minimally affecting the function of MDS HSPCs. In this scenario, the altered microenvironment would confer a relative competitive advantage to MDS HSPCs. Substantive evidence indicates that age- and disease-related microenvironment changes occur in the bone marrow (BM) niche and in the blood of MDS patients. For example, MDS patients exhibit increased inflammatory signaling, including elevated levels of cytokines, chemokines, microbial signals and alarmins[7]. Although inflammatory signaling is important for regulating the function of HSCs, chronic exposure to inflammatory signals can irreversibly impair HSCs[8]. Despite overwhelming evidence of chronic inflammation in MDS[9], the effects of inflammatory signals on MDS HSPCs are not understood.

MDS HSPCs also exhibit dysregulated innate immune signaling converging on key mediators of Toll-like receptor (TLR) signaling. However, MDS-associated mutations lead to the activation of innate immune signaling through various mechanisms, and overexpression and mutations of genes involved in innate immune pathways is reported in over 50% of MDS patients[9]. In deletion (del) 5q MDS HSPCs, haploinsufficiency of chromosome (chr) 5q genes, such as microRNA 146a (MIR146A, hereafter miR-146a), results in activation of the TLR mediator TRAF6 (refs. [10–12]). Activation of TRAF6 in HSPCs results in hematopoietic defects in mouse models[5,10,13–15], suggesting that dysregulation of innate immune-related genes in MDS HSPCs likely contributes to the

pathogenesis of MDS. Here, we investigated the effects of chronic inflammation on the competitive advantage of MDS HSPCs. We found that unlike normal HSPCs, MDS HSPCs had an altered response to chronic inflammation, and that this response contributed to the sustained myelopoiesis of these cells and their competitive advantage compared to normal HSPC.

Results

MDS HSPCs exhibit cell-intrinsic and cell-extrinsic inflam- matory signaling

We chose to investigate TRAF6 as a molecular marker of cell-intrinsic innate immune signaling activation in MDS as dysregulated innate immune pathway activation in MDS HSPCs converges on TRAF6 (ref.[9]), TRAF6 is overexpressed in CD34+ cells from approximately −40% of MDS patients, compared to <15% in $CD34^+$ cells from age-matched healthy individuals[9], and TRAF6 overexpression correlated with worse overall survival in MDS ($P = 0.07$, Extended Data Fig. 1a). To determine whether expression of TRAF6 was correlated with distinct gene regulatory programs and/or molecular alterations in MDS HSPCs, we analyzed publicly available gene expression and genome sequencing data from MDS patients stratified based on the expression of TRAF6 in $CD34^+$ cells. MDS $CD34^+$ cells with high expression of TRAF6 ($Z > 1.0$, hereafter $TRAF6^{hi}$ MDS) were not significantly enriched for particular genetic alterations when compared to MDS $CD34^+$ cells with low expression of TRAF6 ($TRAF6^{10}$ MDS, $Z < -1.0$) (Fig. 1a), suggesting expression of TRAF6 was genetically agnostic in MDS. However, $CD34^+TRAF6^{hi}$ MDS cells had 822 genes differentially expressed (1.5-fold, $P < 0.05$) when compared to $CD34^+TRAF6^{10}$ MDS cells (Fig. 1a and Supplementary Table 1). Gene set enrichment analysis (GSEA) indicated that $CD34^+TRAF6^{hi}$ MDS cells were enriched in inflammatory and immune-related signaling signatures compared to $CD34^+TRAF6^{10}$ MDS cells (Fig. 1b). Furthermore, we examined the expression of inflammatory and immune-related genes in genetically defined subsets of MDS patients. GSEA analysis of TET2 or ASXL1 mutant $CD34^+$ MDS cells stratified on TRAF6 expression revealed that TET2 or ASXL1 mutant $CD34^+TRAF6^{hi}$ MDS cells were also significantly enriched in inflammatory and immune-related signaling signatures as compared to TET2 or ASXL1 mutant $CD34^+TRAF6^{10}$ MDS cells (Fig. 1c). However, BM $CD34^+$ cells from healthy donors did not exhibit enrichment of inflammatory or immune-related genes or pathway signatures when stratified based on high expression of TRAF6 (hypergeometric test, $P = 0.45$). These observations indicate that TRAF6 either directly mediated the expression of genes associated with inflammatory and immune-related signaling in MDS, or, alternatively, $TRAF6^{hi}$ MDS cells reflected a cell-intrinsic response to chronic inflammation in MDS patients.

Although TRAF6 is a critical signaling mediator downstream of various immune receptors[16,17], it is unclear whether TRAF6 overexpression is sufficient to induce the expression of genes associated with inflammatory and immune-related signaling in HSPCs. To investigate the contribution of TRAF6 overexpression and TLR activation in MDS HSPCs, we used transgenic mice that overexpress TRAF6 under the control of hematopoietic-specific *Vav* regulatory elements (called Vav-TRAF6 mice hereafter)[5], and in which the expression of TRAF6 was similar to the levels of TRAF6 overexpression observed

in human CD34$^+$ MDS cells[5]. RNA-sequencing analysis of Lineage$^-$Scal$^+$c-Kit$^+$ (LSK) cells from Vav-TRAF6 and wild-type (WT) mice indicated that TRAF6 overexpression did not induce an inflammatory state in HSPCs (Fig. 1d, Extended Data Fig. 1b,c and Supplementary Tables 2–4). Therefore, we next determined the response of TRAF6-overexpressing HSPCs to low-grade inflammatory signals (Extended Data Fig. 1b). To mimic the inflammatory state observed in MDS patients, we used the gram-negative bacterial component lipopolysaccharide (LPS), a ligand for TLR4, which induces systemic inflammation and affects HSPC function[18]. In vitro treatment with 1 μgml^{-1} of LPS induced the expression of a gene signature associated with an inflammatory state in Vav-TRAF6, but not in WT LSKs, compared to untreated Vav-TRAF6 LSKs (Fig. 1d and Extended Data Fig. 1c). We also deleted miR-146a, a negative regulator of TLR signaling that is frequently deleted in MDS, in human BM CD34$^+$ cells (Extended Data Fig. 1d,e)[11,15,19]. RNA-sequencing analysis indicated that *miR146a*$^{-/-}$CD34$^+$ cells did not exhibit inflammatory signaling at basal state when compared to normal human CD34$^+$ cells (Fig. 1d and Supplementary Tables 5–8). However, treatment with LPS induced the dysregulation of genes associated with an inflammatory state in *miR146a*$^{-/-}$ CD34$^+$ cells to a greater extent than untreated *miR146a*$^{-/-}$CD34$^+$ cells or LPS-stimulated CD34$^+$ cells (Fig. 1d and Extended Data Fig. 1c). The inflammatory state of mouse Vav-TRAF6 LSKs or human *miR146a*$^{-/-}$CD34$^+$ cells in the presence of LPS was similar to that of CD34$^+$TRAF6^{hi} MDS cells (Fig. 1d). These findings indicate that overexpression of TRAF6 in HSPCs was insufficient to directly mediate the expression of inflammatory and immune-related genes, and also that the TRAF6^{hi} MDS cells reflected the cell-intrinsic, TLR-TRAF6-mediated response to extrinsic inflammatory signals.

TLR-TRAF6-primed HSPCs outcompete WT HSPCs in low-dose-LPS conditions

Chronic exposure to LPS irreversibly damages HSC function as defined by decreased competitive transplantation and hematopoietic reconstitution[20–23]. Moreover, LPS can induce adaptations in HSCs and myeloid progenitor cells toward enhanced myelopoiesis[24]. To examine the relative fitness of TLR-TRAF6-primed HSPCs in an inflammatory milieu designed to mimic conditions in aging MDS patients, we performed in vivo BM cell competition assays following chronic low-dose treatment with LPS (1 μg g^{-1}, referred to hereafter as LD-LPS). To avoid a differential response of CD45.2- and CD45.1-expressing hematopoietic cells to LPS, as reported[25], we generated CD45.2 Vav-TRAF6 mice expressing yellow fluorescent protein (YFP) in all hematopoietic lineages (Vav-TRAF6-YFP), which could be distinguished from CD45.2 WT (YFP$^-$) cells (Extended Data Fig. 2a–d). Two months after cotransfer of BM cells from Vav-TRAF6-YFP and WT mice (a one to one ratio) into lethally irradiated CD45.1 WT mice, chimeric mice were injected with LD-LPS or PBS intraperitoneally (i.p.) twice a week for 30 days. PBS-treated chimeric mice had a relative reduction of YFP$^+$ Vav-TRAF6 cells in the peripheral blood (PB) at day 30 (42%) compared to day 0 (before LD-LPS, 51%) (Fig. 2a), consistent with other models of increased TLR-TRAF6 signaling[5,11,15]. LD-LPS chimeric mice exhibited a relative increase of YFP$^+$ Vav-TRAF6 in the PB at day 30 (53%) compared to 47% at day 0 (Fig. 2a). The proportion of YFP$^+$ Vav-TRAF6 cells in the blood of LD-LPS mice at day 30 (53%) was higher compared to 42% at day 30 in PBS mice (Fig. 2a). The proportion of CD11b$^+$ mature myeloid cells was higher among the YFP$^+$ Vav-TRAF6 cells than among YFP$^-$ WT cells in

LD-LPS mice at day 30 (Fig. 2b). YFP$^+$ Vav-TRAF6 cells represented 51% of donor Lin$^-$c-Kit$^+$ (LKs) and 58% of donor Lin$^-$Sca-1$^+$c-Kit$^+$ (LSKs) in the PBS-treated mice at day 30 (Fig. 2c,d), and 65% of LKs and 69% of LSK in LD-LPS mice at day 30 (Fig. 2c,d). These findings indicate that TLR-TRAF6-primed HSPCs exhibited increased myelopoeisis and had a competitive advantage over WT cells during chronic low-grade chronic inflammation.

To investigate the long-term consequences of LD-LPS on TLR-TRAF6-primed HSPCs as compared to WT HSPCs, BM cells from the chimeric mice were isolated at day 30 and serially transplanted into lethally irradiated CD45.1 WT mice, followed by evaluation of the proportions of YFP$^+$ Vav-TRAF6 cells and YFPWT cells among B220$^+$ B cells, CD3$^+$ T cells and CD11b$^+$ myeloid cells every month for 3 months after each of the transplantations (Extended Data Fig. 2a). The proportion of YFP$^+$ Vav-TRAF6 cells derived from the PBS-treated mice decreased from 81% at month 7 to 33% at month 9 after the tertiary BM transplantation (Fig. 2e). In contrast, LD-LPS mice-derived YFP$^+$ Vav-TRAF6 cells maintained high frequencies in the blood of secondary (65%) and tertiary (82%) recipient mice (Fig. 2e), as a result of expanded CD11b$^+$ mature myeloid and CD3$^+$ and B220$^+$ lymphoid cells compared to YFP$^-$ WT cells (Fig. 2e). Consistent with the chimerism in the blood, the proportion of YFP$^+$ Vav-TRAF6 cells among LKs, LSKs and CD150$^+$CD48$^-$LSKs (HSCs) in the BM notably decreased from −50% (month 1) to 23C-20% (month 9) relative to the $^-$FP~ WT cells on tertiary BM transplantation of cells derived from PBS-treated mice (Fig. 2f,g), indicating that TLR-TRAF6-primed HSCs were functionally less competitive than WT HSCs in the absence of exposure to inflammation. In contrast, the proportion of YFP$^+$ Vav-TRAF6 LKs, LSKs and HSCs derived from the LD-LPS mice increased from −50% (month 1) to −95% (month 9) on tertiary BM transplantation (Fig. 2f,g), indicating that TLR-TRAF6-primed HSCs exhibited long-term competitive advantage compared to WT HSCs cells following exposure to low-grade chronic inflammation.

TLR-TRAF6-primed HSPCs undergo myelopoiesis in LD-LPS conditions

We further investigated the effects of chronic low-grade inflammation on the differentiation potential and recovery of TLR-TRAF6-primed HSPCs. Total BM cells isolated from CD45.2 Vav-TRAF6 or CD45.2 WT mice injected i.p. with LD-LPS twice a week for 30 days were washed to remove residual LPS and serially transplanted every 4months with CD45.1 WT competitor BM cells into lethally irradiated CD45.1 WT mice (Extended Data Fig. 3a). Exposure to LD-LPS resulted in reduced proportion (63%) of CD45.2$^+$ WT HSCs (CD150$^+$CD48$^-$LSKs) in the BM compared to PBS-derived CD45.2$^+$ WT HSCs (97%) at month 4 of the secondary BM transplantation (Fig. 3a), consistent with previous reports[22]. By the tertiary competitive BM transplantation, the proportion of LD-LPS-derived CD45.2$^+$ WT HSCs was restored to 80%, comparable to PBS-derived CD45.2$^+$ WT HSCs (80%) at month 4 of the tertiary BM transplantation (Fig. 3a). LD-LPS-derived CD45.2$^+$ Vav-TRAF6 cells also had reduced proportions of HSCs (CD150$^+$CD48$^-$LSKs) in the BM (57%), compared to PBS-derived CD45.2$^+$ Vav-TRAF6 HSCs (94%) at month 4 of the secondary BM transplantation (Fig. 3a), while the proportion of CD45.2$^+$ HSCs was restored (82%) and comparable to that of PBS-derived CD45.2$^+$ Vav-TRAF6 HSCs (89%) at the same time points (Fig. 3a). The frequencies of LD-LPS-derived CD45.2$^+$ WT LKs (80%) and LSKs

(74%) was notably lower compared to PBS-derived CD45.2$^+$ WT LKs (98%) and LSKs (97%) at month 4 of the secondary BM transplantation and remained reduced (54% for LKs and 66% for LSKs) after the tertiary competitive BM transplantation (Fig. 3b,c). Although the proportions of LD-LPS-derived CD45.2$^+$ Vav-TRAF6 LKs (67%) and LSKs (61%) was significantly lower compared to PBS-derived CD45.2$^+$ Vav-TRAF6 LKs (97%) and LSKs (97%) at month 4 of the secondary BM transplantation, the proportion of CD45.2$^+$ Vav-TRAF6 cells from LD-LPS-treated mice among the LKs and LSKs recovered (89% for LKs and 86% for LSKs) by the tertiary competitive BM transplantation (Fig. 3b,c). Among multipotent progenitors, LD-LPS-derived CD45.2$^+$ WT Flk2$^-$CD150$^+$CD48$^+$LSKs (MPP2), Flk2$^-$CD150$^-$CD48$^+$LSKs (MPP3) and Flk2$^+$CD150$^-$CD48$^+$LSKs (MPP4) had low frequencies after the tertiary competitive BM transplantation (Extended Data Fig. 3b). In contrast, LD-LPS-derived CD45.2$^+$ Vav-TRAF6 cells showed a modest expansion of the myeloid-biased MPP2 and the lymphoid-biased MPP4 subsets by the tertiary competitive BM transplantation compared to LD-LPS-derived WT BM cells or PBS-treated Vav-TRAF6 BM cells (Extended Data Fig. 3b). These findings indicate that HSPCs overexpressing TRAF6 recovered after exposure to LD-LPS, while LD-LPS-exposed WT HSPCs showed recovered frequencies of HSCs, but not of hematopoietic progenitor cells.

Next, we tested whether Vav-TRAF6 HSPCs exposed to chronic inflammation maintained durable myeloid cell production. LD-LPS-exposed CD45.2$^+$ WT transplanted BM cells showed a moderate increase in the frequency of CD11b$^+$ mature myeloid cells (42%) after primary competitive BM transplantation (Fig. 3d,e), followed by a decrease in frequency (25%) after the third competitive BM transplantation compared to PBS-treated CD45.2$^+$ WT cells (32% after the primary BM transplantation and 34% after the tertiary transplantation) (Fig. 3d,e). In contrast, the LD-LPS-exposed CD45.2$^+$ Vav-TRAF6 cells represented a higher proportion (75%) of CD11b$^+$ mature myeloid cells after primary competitive BM transplantation compared to LD-LPS-exposed CD45.2 WT cells or PBS-derived Vav-TRAF6 cells (Fig. 3d,e). Moreover, on serial competitive BM transplantation, LD-LPS-exposed Vav-TRAF6 cells represented a higher proportion (64%) of CD11b$^+$ myeloid cells in the recipient mice up to the tertiary BM transplantation (Fig. 3d,e), suggesting that chronic low-grade inflammation enriches for hematopoietic progenitor cells with increased myeloid cell production.

Inflammation activates noncanonical NF-kB in TLR- TRAF6-primed HSPCs

To identify the molecular basis for the competitive advantage of TLR-TRAF6-primed HSPC during low-grade inflammation, we performed RNA sequencing in Vav-TRAF6 and WT LSKs treated with LPS in vitro for 90 min (Fig. 4a). LPS treatment induced 166 differentially expressed genes in Vav-TRAF6 LSKs and 204 differentially expressed genes in WT LSKs compared to untreated Vav-TRAF6 or WT LSKs, respectively (Supplementary Tables 2 and 3). The LPS-treated Vav-TRAF6 LSKs expressed genes associated with inflammatory states that were overwhelmingly represented by signaling through the transcription factor NF-kB (Fig. 4b), which is known to be implicated in loss of quiescence and self-renewal of HSCs in response to inflammatory signaling[26–28]. To validate the activation of NF-kB, we crossed Vav-TRAF6 and WT mice to reporter mice that express a green fluorescent protein (GFP) transgene under the control of three tandem KB-site binding

elements (*cis*-NF-kB^{EGFP})[29]. Vav-TRAF6 NF-kB^{EGFP} Lin^{-} BM cells had increased expression of NF-kB-GFP compared to WT NF-kB^{EGFP} Lin^{-} BM cells after stimulation with LPS (Fig. 4c), suggesting increased activation of NF-kB.

TRAF6 activates the canonical NF-kB pathway, which leads to the NEMO-IKKβ/α-mediated activation of the transcriptional factors RelA-p50, and the noncanonical NF-kB pathway, which leads to the NIK-IKKα-mediated activation of RelB-p52. Although RelA-p50 and RelB-p52 recognize similar kB-site sequences and share an overlapping set of target genes, they also activate distinct set of target genes in a ligand-, cell type- and promoter-dependent manner[30]. Thus, we categorized the inflammatory gene signatures in the LPS-stimulated Vav-TRAF6 and WT LSKs according to canonical and/or noncanonical NF-kB signaling. WT LSKs treated with LPS exhibited enrichment of the canonical NF-kB gene signatures only, while Vav-TRAF6 LSKs treated with LPS were enriched in noncanonical NF-kB gene signatures (Fig. 4b). In addition, Vav-TRAF6 c-Kit^{+} BM cells treated with LPS in vitro had increased expression of p52 and increased nuclear localization of RelB compared to LPS-treated WT c-Kit^{+} BM cells (Fig. 4d).

Next, we determined the enrichment of canonical and noncanonical NF-kB gene signatures in CD34^{+} MDS cells stratified by their expression of TRAF6. CD34^{+}TRAF6^{hi} MDS cells were significantly enriched in CD40 signaling and TNFR2 pathway (noncanonical NF-kB signature), but not TNFR1 pathway and IL-17 pathway (canonical NF-kB signature) compared to CD34^{+}TRAF6^{10} MDS cells (Fig. 4e). Expression of TRAF6 significantly correlated with expression of RelB in CD34^{+}MDS BM cells (Fig. 4f). In addition, we detected an NIK-activated gene signature in LPS-stimulated Va V-TRAF6 LSK and *miR146a*$^{-/-}$CD34^{+} cells compared to untreated WT LSK and CD34^{+} cells, respectively, and increased processing of p100-p52 in CD34^{+} MDS cells compared to WT cells (Extended Data Fig. 4), indicating these cells have increased activation of noncanonical NF-kB. Treatment of CD34^{+} MDS BM cells with a small molecule inhibitor of NIK (NIKi) suppressed nuclear accumulation of RelB (Fig. 4g) and inhibited progenitor colony formation in methylcellulose containing cytokines compared to untreated cells (Fig. 4h). In contrast, NIKi did not affect progenitor colony formation in normal BM CD34^{+} cells at the same or higher doses (Fig. 4h). These findings indicate that MDS HSPCs with increased TLR-TRAF6 priming have activated noncanonical NF-kB signaling.

TLR-TRAF6-primed HSPCs induce A20 expression during inflammation

To identify the mechanism for the shift from canonical NF-kB signaling to noncanomcai NF-kB signaling in TLR-TRAF6-primed HSPC, we compared the gene expression profiles of CD34^{+}TRAF6^{hi} MDS cells, LPS-stimulated human *miR146a*$^{-/-}$CD34^{+} cells and LPS-stimulated Vav-TRAF6 LSKs. Based on all differentially expressed genes in each group (1.5-fold, $P < 0.05$), four genes (*CXCL1*, *CXCL2*, *CXCL3* and *TNFAIP3*) were expressed in all three types of TLR-TRAF6-primed HSPC (Fig. 5a). *TNPAIP3* (which encodes A20) is a target of NF-kB and represses signaling through canonical NF-kB by interfering with the TRAF6, but can simultaneously induce signaling through noncanonical NF-kB by activating NIK[31–33]. A20 messenger RNA expression was significantly increased in CD34^{+}TRAF6^{hi} MDS cells compared to CD34^{+}TRAF6^{10} MDS cells (Fig. 5b). Moreover, LPS stimulation

resulted in a significant increase in A20 mRNA in Vav-TRAF6 LSKs and human *miR146a*$^{-/-}$ CD34^{+} cells compared to LPS-treated WT LSKs and human CD34^{+} cells, respectively (Fig. 5c,d). Expression of A20 was also increased in human *miR146a*$^{-/-}$CD34^{+} cells following treatment with PAM3CSK4 and IL-1β (Fig. 5d), suggesting that a variety of MDS-associated inflammatory signals can increase A20 expression in TLR-TRAF6-primed HSPC. In vitro stimulation with LPS increased the expression of A20 3.4-fold in Vav-TRAF6 c-Kit^{+} BM cells, compared to a two-fold increase in WT c-Kit^{+} BM cells (Fig. 5e). The LPS-induced expression of A20 in Vav-TRAF6 HSPCs coincided with the nuclear accumulation of RelB in these cells (Fig. 5e). Expression of A20 mRNA and protein was increased in Vav-TRAF6 c-Kit^{+} BM cells compared to WT c-Kit^{+} BM cells after in vivo acute administration of LD-LPS (Fig. 5f,g). To determine whether expression of A20 corresponded with the activation of noncanonical NF-kB in human HSPCs, we overexpressed TRAF6 in the TLR4-expressing human monocytic leukemia cell line THP1. TRAF6-overexpressing THP1 cells exhibited increased expression of A20 and a corresponding increase in p52 processing and nuclear RelB 3h post-LPS stimulation compared to vector-expressing THP1 cells stimulated with LPS (Fig. 5h). Thus, activation of noncanonical NF-kB correlates with expression of A20 in TLR-TRAF6-primed HSPCs.

TET2-deficient HSPCs express A20 and activate noncanonical NF-kB

We next investigated whether HSPCs in other subtypes of MDs exhibited increased expression ot A20 and activation ot noncanonical NF-kB. Mutations in TET2, which were detected in TRAF6^{hi} MDS cells (Fig. 1a), have been linked to increased inflammatory signaling[34]. TET2 was reported to resolve inflammation by recruiting HDAC2 to inhibit the TRAF6-mediated expression of inflammatory cytokines[35]. As such, we evaluated the consequences of inflammation on the function of HSPCs from VavCre-Tet2$^{f/f}$ mice (hereafter *Tet2*$^{-/-}$). BM cells isolated from CD45.2 *Tet2*$^{-/-}$ mice on day 30 after daily administration of LD-LPS were cotransferred with CD45.1 WT BM cells into lethally irradiated CD45.1 WT mice. Consistent with previous reports using acute LPS stimulation[36], LD-LPS-exposed CD45.2^{+} *Tet2*$^{-/-}$ cells represented a significantly higher proportion of CD11b^{+} mature myeloid cells after 30 days postcompetitive BM transplantation compared to LD-LPS-exposed CD45.2^{+} WT cells or PBS-derived Tet2cells (Extended Data Fig. 5a). Moreover, LD-LPS-exposed CD45.2^{+} *Tet2*$^{-/-}$ HSPCs (LSKs and HSCs) did not decrease after LPS exposure, while during this time LD-LPS-exposed WT HSPCs decreased as compared to untreated WT HSPCs (Extended Data Fig. 5b), suggesting that TET2 deficiency resulted in increased sensitivity to TLR-TRAF6 stimulation.

To determine whether noncanonical NF-kB was activated in TET2-deficient HSPCs, we performed RNA sequencing on LPS-treated and untreated *Tet2*$^{-/-}$ LSKs (Supplementary Tables 9 and 10), and compared these gene expression changes to those observed in the LPS-treated group. Six genes were differentially expressed (1.5-fold, $P < 0.05$) in LPS-treated *Tet2*$^{-/-}$ LSKs and Vav-TRAF6 LSKs (Fig. 6a), and A20 was among the genes overexpressed in both LPS-stimulated *Tet2*$^{-/-}$ LSKs and Vav-TRAF6 LSKs (Fig. 6a). LPS stimulation resulted in a significant increase in A20 mRNA in *Tet2*$^{-/-}$ LSKs compared to nonstimulated *Tet2*$^{-/-}$ LSKs and WT LSKs (Fig. 6b), and the enrichment of a gene expression signatures found in CD34^{+}TRAF6^{hi} MDS cells (Fig. 6c). LPS treatment resulted

in enrichment of CD40 signaling (noncanonical NF-kB) in *Tet2*$^{-/-}$ LSKs and enrichment of TNFR1 pathway (canonical NF-kB) in WT LSKs (Fig. 6d). *Tet2*$^{-/-}$ c-Kit^{+} BM cells treated with LPS in vitro had increased expression of A20 and p52 proteins, and increased nuclear localization of RelB compared to LPS-treated WT c-Kit^{+} BM cells (Fig. 6e). Next, we bred Traf6$^{f/f}$ and VavCre-Tet2$^{f/f}$ mice to delete the expression of TRAF6 in HSPCs (hereafter *Tet2*$^{-/-}$*Traf6*$^{-/-}$) (Extended Data Fig. 6). *Tet2*$^{-/-}$*Traf6*$^{-/-}$ c-Kit^{+} cells did not induce the expression of A20 and/or nuclear localization of RelB after LPS stimulation (Fig. 6f). Expression of A20 mRNA and protein was also increased in c-Kit^{+} BM cells isolated from *Tet2*$^{-/-}$mice after administration of LD-LPS compared to WT c-Kit^{+} BM cells (Fig. 6g,h). These observations indicate that TET2-deficient HSPCs were primed for TLR-TRAF6 activation and had activated noncanonical NF-kB during low-dose inflammation.

A20 deletion suppresses noncanonical NF-kB in TLR-TRAF6- primed HSPCs

Next, we tested the requirement for A20 in the activation or noncanomcal NF-kB, myeloid-biased hematopoiesis and competitive advantage during inflammation in TLR-TRAF6-primed HSPCs. LPS stimulation of THP1 cells expressing short-hairpin RNAs targeting A20 diminished the expression of p52, reduced the nuclear localization of RelB and increased the nuclear localization of RelA (Fig. 7a). We also bred RosaCreER A20$^{f/w}$ mice to Vav-TRAF6 mice to delete A20 on tamoxifen-induced recombination (hereafter A20$^{+/-}$Vav-TRAF6) (Extended Data Fig. 7). Similarly, c-Kit^{+} BM cells from A20$^{+/-}$Vav-TRAF6 had near-complete inhibition of p52 expression and the nuclear localization of RelB (Fig. 7b), indicating that A20 maintained signaling through noncanonical NF-kB in human and mouse TLR-TRAF6-primed HSPCs.

Next, we compared the effect of LD-LPS in CD45.1 WT mice reconstituted with equal mixes of CD45.2 UBC-GFP^{+} WT (WT-GFP) and CD45.2 Vav-TRAF6 or CD45.2 Vav-TRAF6 RosaCreER A20$^{f/w}$ BM cells and treated with tamoxifen to delete one copy of A20 (hereafter A20$^{+/-}$Vav-TRAF6). Sixty days postengraftment and ~80 days posttamoxifen treatment, chimeric mice were injected i.p. with LD-LPS or PBS twice a week for 4 weeks. At this timepoint, we observed an increase in the relative frequency of CD45.2^{+}GFPVav-TRAF6 cells compared to that of CD45.2^{+}GFP^{+} WT cells in the blood of chimeric mice treated with LD-LPS compared to PBS-treated chimeric mice (Fig. 7c). In contrast, the relative frequency of CD45.2^{+}GFP^{-} A20$^{+/-}$Vav-TRAF6 cells to that of CD45.2^{+}GFP^{+} WT cells decreased in chimeric mice treated with LD-LPS compared to those treated with PBS (Fig. 7c). To investigate whether reducing A20 would mitigate the myeloid-biased hematopoiesis induced by inflammation in TLR-TRAF6-primed HSPCs, BM cells from CD45.2 Vav-TRAF6, A20$^{+/-}$Vav-TRAF6 or WT mice injected i.p. with LD-LPS twice a week for 4 weeks were transplanted together with competitor CD45.1 WT BM cells into lethally irradiated CD45.1 WT mice. Exposure to LD-LPS resulted in a sustained increase of CD45.2^{+}CD11b^{+} Vav-TRAF6, but not A20$^{+/-}$Vav-TRAF6 myeloid cells compared to CD45.2^{+}CD11b^{+} WT cells (Fig. 7d). These findings indicate that the competitive advantage and increased myelopoiesis in TLR-TRAF6-primed HSPCs is mediated by A20 expression.

Last, to investigate whether human MDS cells required A20 for clonogenic potential, we used a cell line derived from an MDS patient (MDSL)[37] expressing shRNAs targeting A20

(shA20) or scrambled shRNA control (shControl) (Fig. 7e and Extended Data Fig. 8a). shA20-MDSL cells had a significantly reduced clonogenic potential compared to shControl-MDSL cells when plated into methylcellulose containing SCF, IL-3, erythropoietin and GM-CSF (Fig. 7f and Extended Data Fig. 8b). A similar reduction in clonogenic potential was observed in the AML cell line THP1 following knockdown of A20 (Extended Data Fig. 8c,d). The deubiquitin (DUB) function of A20 is primarily responsible for suppressing signaling through canonical NF-kB[31]. The E3 ligase function and ubiquitin-binding domain of A20 are mediated by the zinc fingers 4 and 7, respectively, which control the stability of RIPK1 protein and the activation of noncanonical NF-kB[31]. Expression of WT A20 rescued the progenitor function of shA20-MDSL cells in methylcellulose (Fig. 7e,f), while expression of $A20^{C103S}$, which cannot repress canonical NF-kB, or $A20^{ZF4/7}$, which cannot activate noncanonical NF-kB, did not restore the progenitor function of shA20-MDSL cells (Fig. 7e,f). These findings indicate that A20 expression in MDS progenitor cells dampened canonical NF-kB signaling and activated noncanonical NF-kB signaling.

Discussion

Here, we show that an inflamed environment was critical for the competitive advantage of MDS HSPCs and for disease progression, particularly in a cohort of MDS patients in which TLR-TRAF6 signaling is activated. We found that TLR-TRAF6-primed HSPCs had altered responses to chronic inflammation, and that these responses, which involved expression of A20 and signaling through the noncanonical NF-kB pathway, contributed to sustained myeloid expansion and endowed these cells with a competitive advantage over WT cells. These findings indicate that low-grade inflammation in MDS patients is a key determinant of the relative long-term competitiveness of the MDS HSPCs.

Unraveling the effects of systemic chronic inflammation in MDS is complicated, because TLRs and downstream effectors of TLR signaling are overexpressed and constitutively activated in MDS HSPCs of over half of MDS patients[9]. TRAF6, a ubiquitin ligase that mediates signaling from several innate immune receptors, is a central mediator of TLR signaling in MDS. Not only is *TRAF6* mRNA overexpressed in ~40% of MDS HSPCs, but also negative regulators of TRAF6 are deleted and/or repressed in MDS HSPCs[10,11,15,38]. Cell-intrinsic TLR-TRAF6 activation results in impaired HSPC function and attrition of HSCs in mouse models[5,11,19,39], suggesting that activation of TLR-TRAF6 signaling alone is not responsible for competitive advantage of MDS HSPCs. These findings indicate that dysregulation of innate immune-related genes is common MDS HSPC, but that additional factors are required to recapitulate the range of pathogenic features of MDS.

Commonly mutated genes in MDS can co-opt the innate immune pathway in HSPCs[9]. TET2 inhibits the expression of proinflammatory cytokines and interferons in immune cells, in part due to repression of TRAF6 signaling[35,40,41]. Consistent with these findings, we found that $Tet2^{-/-}$ HSPC responded to chronic inflammation by increasing myelopoiesis and activating noncanonical NF-kB in a manner dependent on TRAF6. Mutations in DNMT3A have been implicated in regulating innate immune and inflammatory signaling[42,45], yet the precise mechanism by which they lead to increased innate immune signaling remains undetermined. Mutations in RNA splicing factors generate RNA isoforms that directly impact innate

immune signaling[44–46]. For example, mutations in U2AF1 result in expression of an IRAK4 isoform that encodes a protein that associates with MyD88 and leads to activation of NF-kB[45]. Because canonical NF-kB activation impairs the function of normal HSPCs, our data indicate that the shift from canonical to noncanonical NF-kB activation in MDS HSPCs may protect these cells from the consequences of an inflammatory environment. A shift in response to inflammatory signals has been reported in normal biological contexts. Exposure to perinatal alarmins induces the reprogramming of innate immune cells in newborn infants to protect from sepsis by using distinct TLR4 pathways. Neonatal immune cells exposed to alarmins are programmed to activate TRIF-dependent gene programs rather than MyD88-dependent programs downstream of TLR4 (ref. [47]). In contrast, adult innate immune cells use MyD88-dependent gene programs instead of TRIF-dependent programs following TLR4 stimulation. Disruption of this critical reprogramming of TLR pathways increases the risk of hyperinflammation and sepsis in newborns.

Basal expression of A20, a dual-ubiquitin editing protein, is low in most cells, but its expression is rapidly induced on NF-kB activation. The DUB activity of A20 removes K63-linked ubiquitin chains from TRAF6, a modification that terminates the activation of canonical NF-kB by TLRs. A20 also inhibits the activation of canonical NF-kB induced by TAK1, thus A20 suppresses NF-kB activation by multiple mechanisms. The E3 ligase function of A20 targets RIP1 for proteasomal degradation and prevents it from acting as a mediator of inflammatory and necroptosis signaling. A20 also contains a ubiquitin-binding domain that is implicated in activating noncanonical NF-kB signaling by dissociating TRAF2-TRAF3 interactions, which results in stabilization of NIK and increased expression of p52 (ref.[31]). Our studies focused on A20, however, we also observed increased expression of *CXCL2* in Vav-TRAF6 and TET2-deficient HSPCs following LPS treatment. CXCL2 is also an NF-kB target gene and its increased expression may contribute to functional defects of myeloid cells in MDS[48]. Collectively, our data indicate that TLR-TRAF6-mediated A20 expression suppresses canonical NF-kB, likely through its DUB domain, while simultaneously activating noncanonical NF-kB through the Ub-binding domain. Thus, therapies A20 or the noncanonical NF-kB pathway may increase the sensitivity of MDS HSPCs to the inflammatory environment and result in loss of clonal dominance.

Methods

Additional information can be found in the Nature Research Reporting Summary.

Materials

LPS (L6529) and LPS-EB Ultrapure (TLRL-PEKLPS) were purchased from Sigma and InvivoGen, respectively. NIK SIM1 (HY-112433) was purchased from Med Chem Express.

MDS patient and healthy control samples

BM mononuclear cells from MDS patients were obtained from the MD Anderson Cancer Center (G. Garcia-Manero) and University of Cincinnati (Z. Gul). The clinical parameters of the patients were shown in Supplementary Table 11. Healthy control BM samples were obtained from Translational Core Laboratory in Cincinnati Childrens Hospital Medical

Center under an approved Institutional Review Board protocol. The MDS patient samples used in this study were obtained from patients diagnosed with MDS after written informed consent under approval by the Institutional Review Board at the MD Anderson Cancer Center. The study is compliant with all relevant ethical regulations regarding research involving human participants.

Mice

Generation of Vav-TRAF6 mice was described in our previous study[5]. To distinguish CD45.2$^+$ cells based on YFP expression, Vav-TRAF6 mice were crossed to mice expressing a Cdc42-YFP transgene that results in ubiquitous YFP expression. Tet2$^{fl/fl}$ mice (Jackson Laboratory, 017573) and Traf6$^{fl/fl}$ mice[14] were crossed with VavCre mice (Jackson Laboratory, 008610). A20$^{fl/fl}$ mice were kindly provided by A. Ma and described elsewhere[49]. For conditional deletion of A20, A20$^{fl/fl}$ mice were crossed with RosaCreER mice. UBC-GFP mice (Jackson Laboratory, 004353) were purchased from the Jackson Laboratory. NF-kB-GFP reporter mice were generously provided by C. Jobin[29]. All mice were bred, housed and handled in the Association for Assessment and Accreditation of Laboratory Animal Care-accredited animal facility of Cincinnati Childrens Hospital Medical Center.

Hematological analysis

Blood counts were measured with the Genesis blood analyzer (Oxford Scientific).

BM transplantation

For noncompetitive BM transplantations, 1 × 10^6 CD45.2$^+$ BM cells were transplanted into lethally irradiated recipient mice (CD45.1$^+$ B6.SJL$^{PtprcaPep3b/Boy}$, 6–10 weeks of age). For competitive transplantation, BM cells from 8-week-old recipient mice were transplanted into lethally irradiated recipient mice with CD45.1$^+$ B6.SJL$^{PtprcaPep3b/Boyr}$ BM cells or CD45.2$^+$ C57BL/6-Tg(UBC-GFP)30Scha/J BM cells. For serial transplantation, BM cells were collected from all recipient mice 3 months after transplantations, pooled together and then 2 × 10^6 BM cells were transplanted into lethally irradiated recipient mice (CD45.1$^+$ B6.SJL$^{PtprcaPep3b/Boy}$, 6–10 weeks of age).

Flow cytometry

For immunophenotypic analysis of lineage positive cells, PB, BM and spleen samples were processed with 1× red blood cell lysis buffer, and then incubated with CD11b-PE-cy7 (25–0112-81, eBioscience), Gr1-eFluor450 (48–5931-82, eBioscience), CD3-PE (12–0031-83, eBioscience) and B220-APC (17–0452-82, eBioscience). To distinguish donor from recipient hematopoietic cells, PB were stained with CD45.1-Brilliant Violet 510 (110741, BioLegend), and CD45.2-APC-eFluor780 (47–0454-82, eBioscience) or CD45.2-eFluor450 (48–0454-82, eBioscience). For HSPC analysis, BM cells were washed and incubated for 30min with biotin conjugated lineage markers (CD11b, Gr1, Ter119, CD3, B220, mouse hematopoietic lineage biotin panel (88–7774-75 eBioscience)), followed by staining with streptavidin eFluor780 (47–4317-82, eBioscience), Sea-1-PE (12–5981-82, eBioscience), c-Kit-APC (17–117181, eBioscience), Flk2-PE-Cy5 (15–1351-81, eBioscience), CD150-PE-

Cy7 (115914, BioLegend) and CD48-FITC (11–0481-85, Affymetrix) or CD48-eFluor450 (48–0481-80, eBioscience). SLAM-HSC were identified based on expression of $Lin^{-}Sca^{-}1^{+}c\text{-}Kit^{+}CD150^{+}CD48^{-}$. MPP2, MPP3 and MPP4 were identified based on expression of $Lin^{-}Sca–1^{+}c\text{-}Kit^{+}Flk2^{-}CD150^{+}CD48^{+}$, $Lin^{-}Sca^{-}1^{+}c\text{-}Kit^{+}Flk2^{-}CD150^{-}CD48^{+}$ and $Lin^{-}Sca^{-}1^{+}c\text{-}Kit^{+}Flk2^{+}CD150^{-}CD48^{+}$, respectively.

Colony forming assay

$CD34^{+}$ BM cells were purified from MDS BM cells using a CD34 microbeads kit (130–046-702, Miltenyi Biotec). Seven hundred and fifty BM cells per replicate were plated in methylcellulose (H4434, Stemcell Technologies) containing 40 μg ml^{-1} of human plasma-derived low-density lipoprotein (02698, Stemcell Technologies). Colonies were scored at day 14 using STEMvision (22006, Stemcell Technology) according to the manufacturer s protocol.

Immunoblotting

Cell extract was prepared bv lysing cells in SDS sample buffer followed by incubation with benzonase (70746, Millipore) on ice for 10 min. Nuclear and cytoplasmic fractionation was performed with Nuclear Extract Kit (40010, Active Motif) according to the manufacturers protocol. Samples were boiled at 95 °C for 5 min and loaded to SDS-PAGE and electrotransferred to nitrocellulose membranes (162–0112, Bio-Rad). Immunoblot analysis was performed with the following antibodies: TRAF6 (sc-7221, Santa Cruz), A20 (5630, Cell Signaling), NF-kB2 p100/p52 (4882, Cell Signaling), RelA/p65 (8242, Cell Signaling), RelB (sc-226, Santa Cruz), Vinculin (13901, Cell Signaling), glyceraldehyde 3-phosphate dehydrogenase (GAPDH) (5174, Cell Signaling), α/β-Tubulin (2148, Cell Signaling), Lamin B1 (12586, Cell Signaling) and Histone H3 (abl791, Abeam). For capillary immunoassays, cell extracts were prepared by lysing cells in RIPA buffer. The analysis was performed on a JESS system (ProteinSimple) according to the manufacturers instructions using a 12–230kDa Separation Module (AM-PN01, ProteinSimple) and the Anti-Rabbit Detection Module (DM-001, ProteinSimple).

Quantitative RT-PCR

Total RNA was extracted and purified using Quick-RNA MiniPrep (Zymo Research, R1055) or RNeasy Micro Kit (Qiagen), and reverse transcription was carried out using Superscript complementary DNA Synthesis Kit (Invitrogen) or High-Capacity cDNA Reverse Transcription Kit (ThermoFisher). Quantitative RT-PCR was performed with Taqman Master Mix (Life Technologies) for murine Tnf (Mm00443260_g1), 11–6 (Mm00446190_m1), 11-μ(3 (Mm01336189_m1), Tnfaip3/A20 (Mm00437121_m1), Gapdh (Mm99999915_g1), human TNFAIP3/A20 (Hs00234713_m1) and GAPDH (Hs02758991_g1). For quantitative RT-PCR analysis of hsa-miR-146a, RNA was extracted using Quick-RNA MiniPrep (Zymo research, R1055) and reverse transcription was carried out using TaqMan MicroRNA Reverse Transcription Kit (Applied Biosystems, 4366596). Quantitative RT-PCR was performed with TaqMan MicroRNA Assay for human hsa-miR-146a (000468) and human U18 (001204).

Transfection

Transfections in human embryonic kidney-293T (HEK293T) cells were performed with TransIT-LT1 Transfection Reagent (MIR2305, Mirus) according to the manufacturers recommendation.

Virus infection

Doxycycline inducible knockdown of human A20 was performed with shRNAs targeting A20 expressed from pTRIPZ vector (RHS4696–200756146, OpenBiosystems). The leukemic cell lines transduced with pTRIPZ were generated by infection with the supernatants from transfected HEK293T cells in the presence of 4 $\mu g ml^{-1}$ of polybrene (sc-134220, Santa Cruz). After transduction of pTRIPZ, 1 μg of puromycin was used for selection. Doxycycline was used to induce knockdown of A20. Nonsilencing shRNA control (RHS4743) was purchased from Dharmacon. pLKO.1-puro was used for generating THP1-shA20 leukemic cell line as previously described[50]. shA20 and shControl were obtained from viral vector core at Cincinnati Childrens Hospital Medical Center. For overexpression of A20 WT and mutants, MSCV-pGK-GFP vector was used as previously described[26].

Single-guide RNA design and synthesis

Protospacer sequence for human miR-146a was identified using the web tool, CRISPOR (http://crispor.tefor.net/crispor.py)[51]. The targeted sequence of the genomic RNA (sg-miR-146a) is GCTTTGAGAACTGAATTCCA. The gRNA targeting human miR-146a as well as non-targeting gRNA (sg-CTL) were obtained from Synthego.

Cas9-sgRNA precomplexing and transfection

To obtain Cas9-sgRNA RNPs, 45 pmol of synthetic sgRNA (sg-CTL or sg-miR-146a) was incubated with 20pmol of 2NLS Cas9 nuclease (Synthego) for 10 min at room temperature. Human $CD34^+$ BM cells (1×10^6 cells) were electroporated in Buffer R (ThermoFisher). Electroporation was performed using the Neon Transfection System for three pulses at 1,600 V for 10 ms.

RNA sequencing

Total RNA was extracted from the cells using RNeasy Plus Micro Kit (Qiagen). The initial amplification step for all samples was done with the NuGEN Ovation RNA-Seq System v.2. The assay was used to amplify RNA samples to create double-stranded cDNA. The concentrations were measured using the Qubit dsDNA BR assay. Libraries were then created for all samples using the Illumina protocol (Nextera XT DNA Sample Preparation Kit). The concentrations were measured using the Qubit dsDNA HS assay. The size of the libraries for each sample was measured using the Agilent HS DNA chip. The concentration of the pool was optimized to acquire at least 15–20 million reads per sample. Paired-end FASTQ files were aligned to hg38 (human) or mm 10 (mouse) genomes using HISAT2 (http://www.ccb.jhu.edu/software/hisat) or Tophat (https://ccb.jhu.edu/software/tophat). Raw counts were calculated using featureCounts (http://subread.sourceforge.net/) and downstream analysis was performed with iGeak[52]. All RNA-sequencing data generated in this study is available at GSE142560.

Publicly available data

Published microarray data of patients with MDS were obtained from Gene Expression Omnibus series GSE19429 and GSE58831 (refs.[53,54]). Mutation data of MDS patients was obtained from Gerstung et al.[54]. RNA-sequence data of HSPC with constitutive activation of NIK was obtained from GSE88949 (ref.[54]).

GSEA and hypergeometric tests

GSEA was performed as previously described[55]. BM $CD34^+$ cells from patients with MDS were stratified based on low and high TRAF6 expression as defined by: TRAF6 high, $Z > 1.0$; TRAF6 low, $Z < —1.0$. Differentially expressed genes (1.5-fold, $P < 0.05$) were identified in 'TRAF6 high[5] MDS $CD34^+$ cells relative to 'TRAF6 low' MDS $CD34^+$ cells ($n = 822$) (Supplementary Table 1). GSEA was then performed on 'TRAF6 high' versus 'TRAF6 low' MDS $CD34^+$ cells. For examination of inflammatory and immune-related GSEA and differential gene expression changes in healthy donor BM cells, TRAF6 (205558_at) expression from GSE58831 was stratified based on 'TRAF6 high' ($Z > 1.0$) and TRAF6 low' ($Z < — 1.0$) expression. Using all genes ($n = 530$) from the inflammatory and immune-related GSEA pathways (Fig. 1b and Extended Data Fig. 1b), enrichment of differentially expressed genes in MDS ($n = 159$) and healthy donor cells (n = 17) was calculated by the hypergeomtric tests. Upregulated (two-fold, $P< 0.001$) genes in the 'TRAF6 high' group from healthy donors' BM hematopoietic cells did not exhibit significant enrichment of inflammatory or immune-related gene expression or pathway signatures (hypergeometric test, $P = 0.45$) when stratified based on higher TRAF6 expression ($Z >1.0$). Using the same analysis, upregulated (two-fold, $P < 0.05$) genes in 'TRAF6 high' MDS cells were significantly enriched in inflammatory and immune-related genes (hypergeometric test, $P =9.0 \times 10^{-18}$).

Statistical analysis

Unless otherwise specified, results are depicted as the mean ± s.d. Statistical analyses were performed using Students *t*-test. For KaplanMeier analysis, the Mantel-Cox test and hypergeometric test were used. GraphPad Prism (v.5, GraphPad) was used for statistical analysis. For correlative analyses, Spearmans rank test was used.

Reporting Summary

Further information on research design is available in the Nature Research Reporting Summary linked to this article.

Extended Data

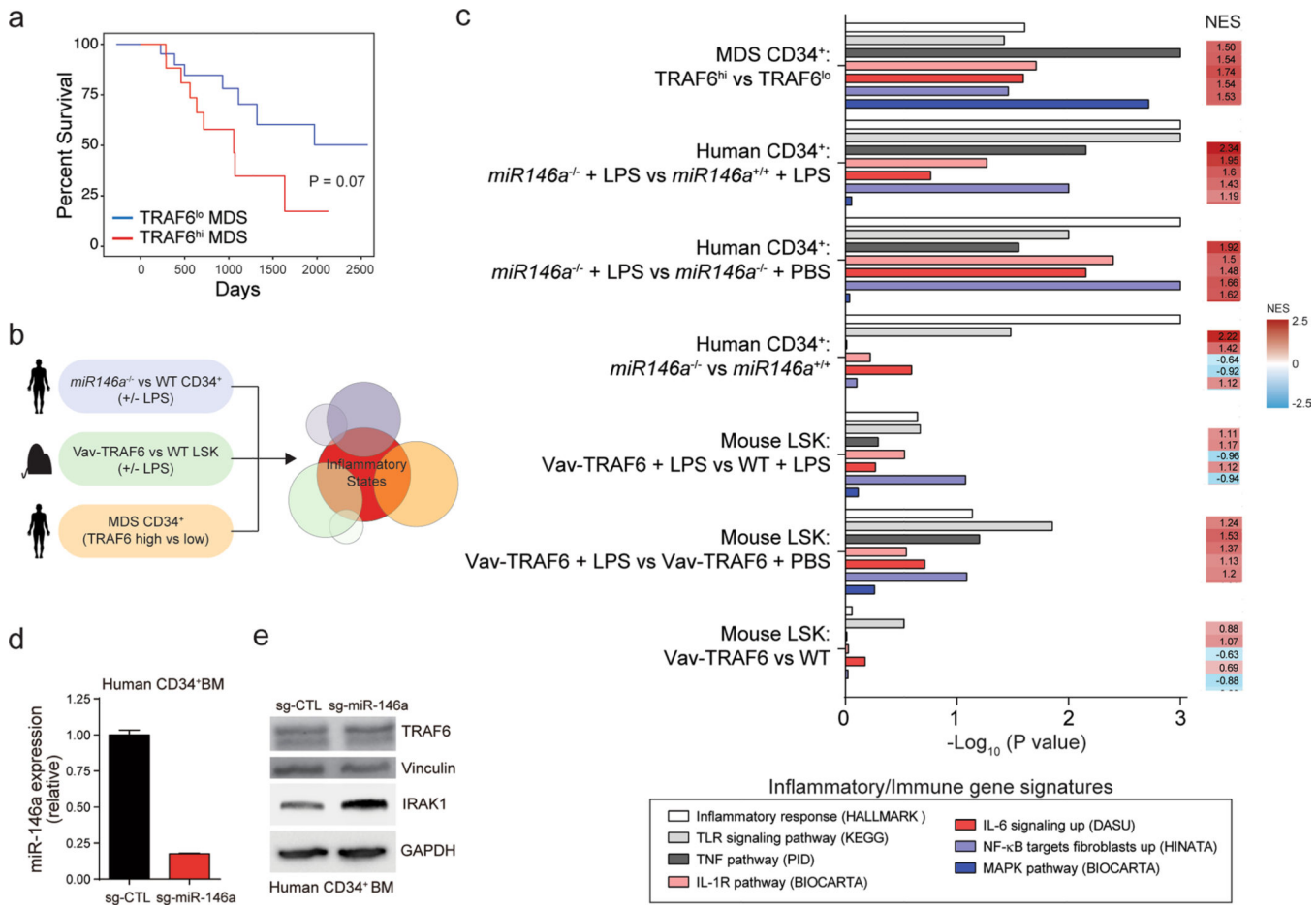

Extended Data Fig. 1 |. Inflammatory and immune pathway activation in MDS cells.

a, Survival analysis of MDS patients based on TRAF6 expression (probe: 227264_at) in $CD34_+$ cells (GSE58831). Patients were stratified based on TRAF6 mRNA expression (top 20%, n = 28; bottom 20%, n = 26). Log-rank (Mantel-Cox) test. **b**, Overview of experimental design to examine inflammatory states in MDS and human TLR-TRAF6 primed HSPC. **c**, Human miR-146a deficient (*miR146a*$^{-/-}$) and control (WT) $CD34^+$ BM cells generated from healthy $CD34^+$ BM using CRISPR-Cas9 gene editing or Vav-TRAF6 and WT LSK BM cells were stimulated in vitro for 90 min with 1μg/mL of LPS (or PBS) (n = 3 each per group) and then examined for differential gene expression by RNA-sequencing. The inflammatory state for each group was determined using the GSEA. NES, normalized enrichment score. **d**, Expression of miR-146a in miR-146a deficient (*miR146a*$^{-/-}$) and control (sg-CTL) $CD34^+$ BM cells gene edited using CRISPR-Cas9. Results are presented as mean ± s.e.m. for n = 3 technical replicate samples. **e**, Immunoblot analysis of TRAF6 and IRAK1, two miR-146a targets, in *miR146a*$^{-/-}$ and control (sg-CTL) $CD34^+$ BM cells gene edited using CRISPR-Cas9. Shown is an immunoblot from a single biological replicate.

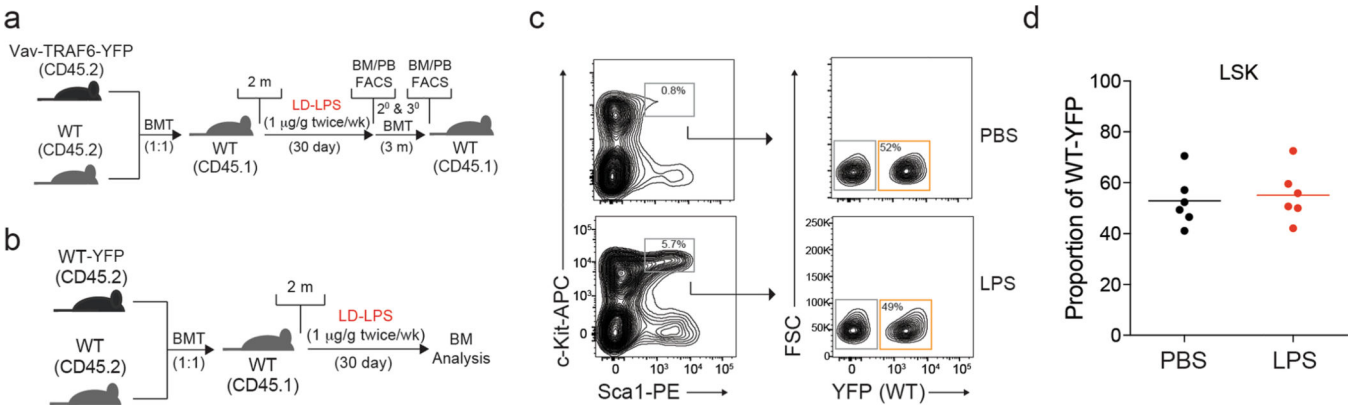

Extended Data Fig. 2 |. Evaluation of Vav-TRAF6-YFP and WT-YFP versus WT BM cell competition with LD-LPS.

a, Overview of experimental design to directly measure hematopoietic cell competition in the presence of low-dose chronic inflammation. Vav-TRAF6 CD45.2 BM cells (co-expressing a YFP transgene referred to as Vav-TRAF6-YFP) and WT CD45.2 BM cells were transplanted in equal proportions into lethally irradiated recipient mice. Two months after transplantation, chimeric mice were treated with LD-LPS (1 μg/g) or vehicle twice a week for 30 days and then examined for hematopoietic contribution of Vav-TRAF6-YFP and WT cells in the PB and BM. After the last LPS treatment, BM cells were serially transplanted into lethally irradiated recipient mice. **b**, Overview of experimental design to directly measure hematopoietic cell competition in the presence of low-dose chronic inflammation. Wild-type (WT) CD45.2 BM cells (co-expressing a YFP transgene) and WT CD45.2 BM cells were transplanted in equal proportions into lethally irradiated recipient mice. Two months after transplantation, chimeric mice were treated with LD-LPS (1 μg/g) or vehicle twice a week for 4 weeks and then examined for hematopoietic contribution of WT-YFP and WT cells in the BM. **c**, Representative flow cytometric profiles and gating strategy of YFP^+ (WT-YFP) cells in the BM of chimeric mice after LPS or vehicle (PBS) treatment. **d**, The proportion of YFP^+ (WT-YFP) cells in LSK populations 4 weeks after treatment with LPS or vehicle (PBS). Data represent the mean ± s.e.m., n = 6 mice per group.

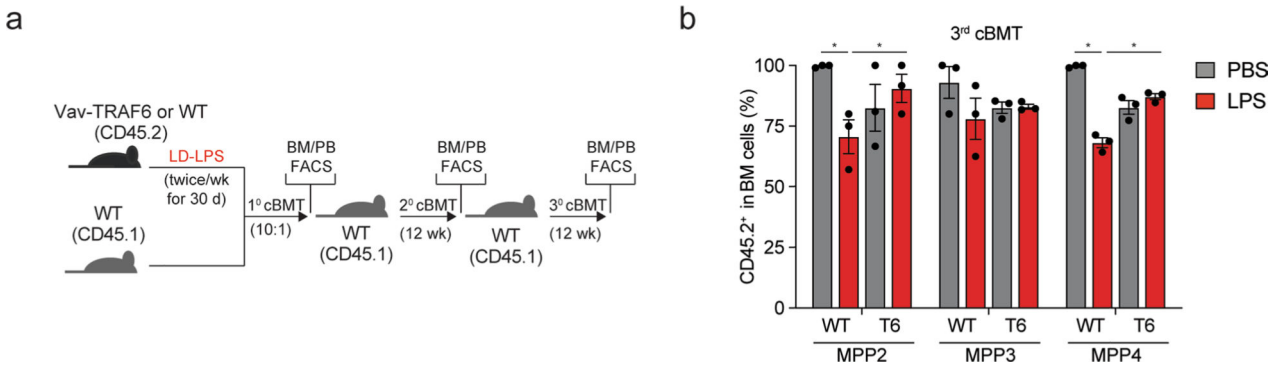

Extended Data Fig. 3 |. Overexpression of TRAF6 alters the response of hematopoietic progenitor cells to LD-LPS.

a, Overview of experimental design to examine the long-term effects of low-dose chronic inflammation on hematopoiesis. Vav-TRAF6 (T6) CD45.2 BM cells or WT CD45.2 BM cells were isolated from mice treated with LD-LPS (1 μg/g) or vehicle twice a week for 30 days and then transplanted with a ratio of 10:1 of CD45.1 competitor BM cells into lethally irradiated recipient mice. Three months after transplantation, BM cells were serially transplanted into lethally irradiated recipient mice. **b**, The proportion of donor-derived $CD45.2^+$ cells in MPP2 ($Flk2^-CD150^+CD48^+LSK$), MPP3 ($Flk2^-CD150^-CD48^+LSK$), and MPP4 ($Flk2^+CD150^-CD48^+LSK$) after tertiary transplantation. Results are presented as mean ± s.e.m. for n = 3 mice per group. Statistical analysis was performed by a two-tailed Student's t-test. *, $P < 0.05$.

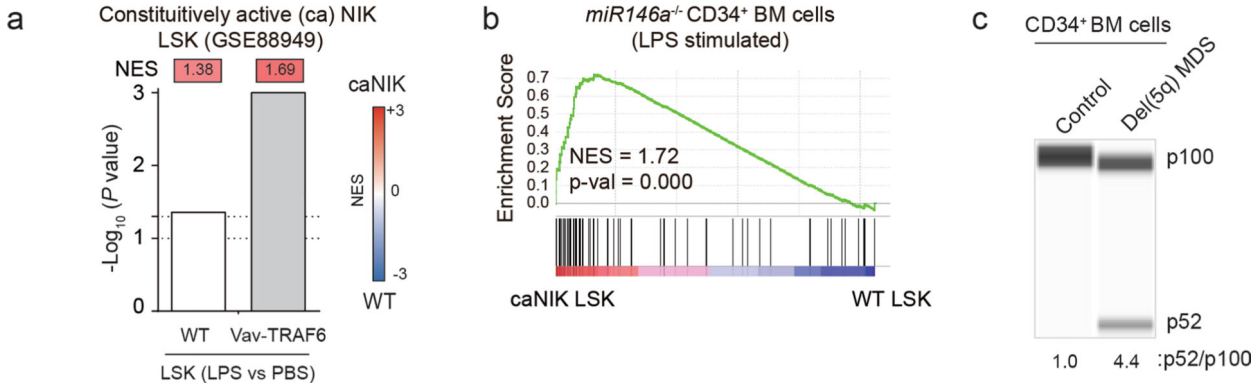

Extended Data Fig. 4 |. TLR-TRAF6 primed HSPC exhibit expression of non-canonical NF-kB gene signatures.

a, Normalized enrichment scores (NES) and P value of gene signatures established from WT and Vav-TRAF6 LSK stimulated with LPS evaluated in constitutively active (ca) NIK expressing LSK (GSE88949). **b**, GSEA plots established from caNIK LSK were evaluated in miR-146a deficient (*miR146a*$^{-/-}$) CD34^{+} BM cells gene edited using CRISPR-Cas9 and then stimulated with 1 μg/mL of LPS (or PBS) for 90 min. The gene expression profiles are relative to unstimulated miR146a$^{-/-}$ CD34^{+} BM and control (sg-CTL) (+/- LPS). (**c**) Capillary immunoassay of CD34^{+} cells isolated from healthy controls or MDS BM visualized by chemiluminescence using ProteinSimple. Shown is an immunoassay from a single biological replicate.

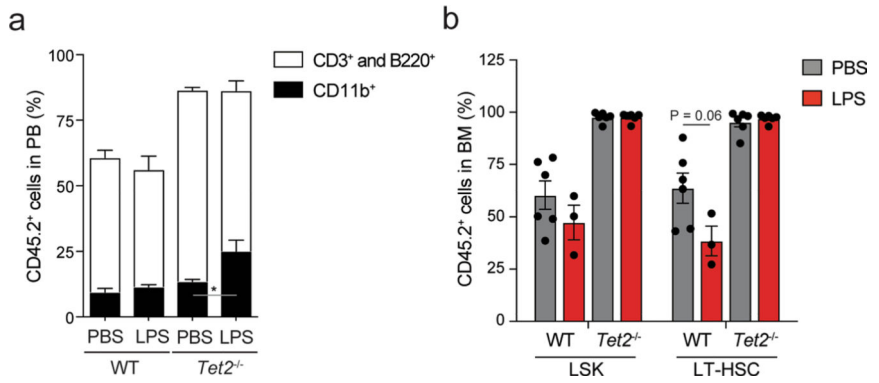

Extended Data Fig. 5 |. TET2 deficiency in hematopoietic cells results in increased myeloid-biased hematopoiesis without affecting the proportions of HSC after LD-LPS.

a, Overview of experimental design to examine the effects of low-dose chronic inflammation on hematopoiesis. $Tet2^{f/f}$ VavCre CD45.2 BM cells ($Tet2^{-/-}$) or $Tet2^{f/f}$ (WT) CD45.2 BM cells were isolated from mice treated with LD-LPS (1 μg/g) or vehicle twice a week for 4 weeks and then transplanted into lethally irradiated recipient mice (along with CD45.1 competitor BM cells). One month after transplantation, PB and BM cells were evaluated by flow cytometry. **b**, The proportion of donor-derived $CD45.2^+$ myeloid ($CD11b^+$) and lymphoid (B220+ and $CD3^+$) cells in the PB (n = 6 mice per group). * P = 0.02. **c**, The proportion of donor-derived $CD45.2^+$ LSK and LT-HSC in the BM of mice after treatment with LD-LPS. Results are presented as mean ± s.e.m., n = 6 for all groups; n = 3 for WT LPS treated group. * P = 0.03. Statistical analysis in b was performed by a two-tailed Student's t-test. Statistical analysis in **c** was performed by a one-tailed Student's t-test.

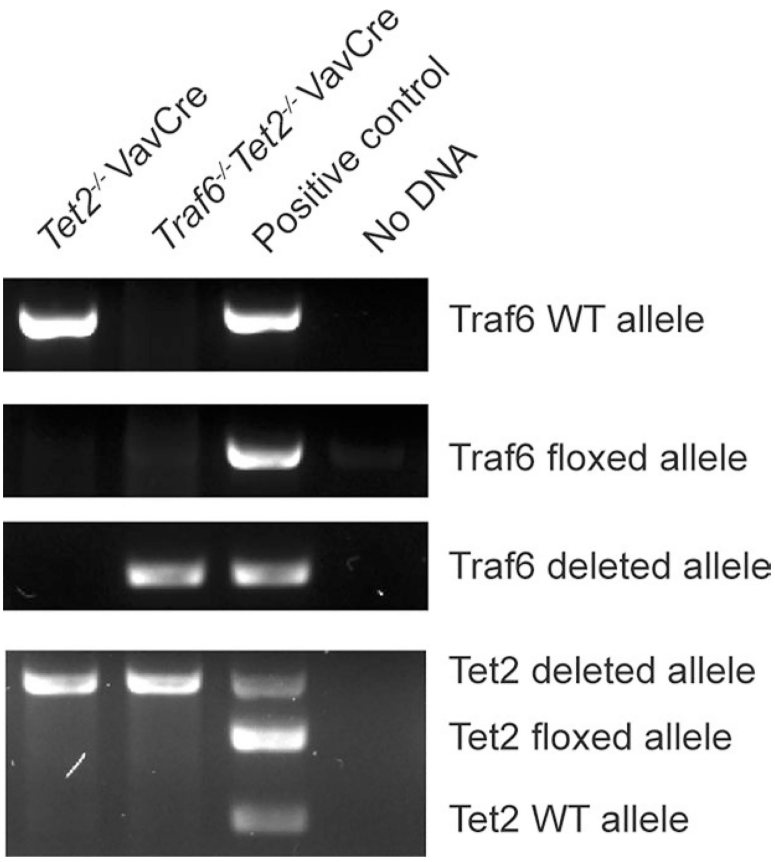

Extended Data Fig. 6 |. Generation of Traf6- and Tet2-deficient mice.
Genotyping analysis of $Tet2^{-/-}$ VavCre and $Traf6^{-/-}$ $Tet2^{-/-}$ VavCre mice.

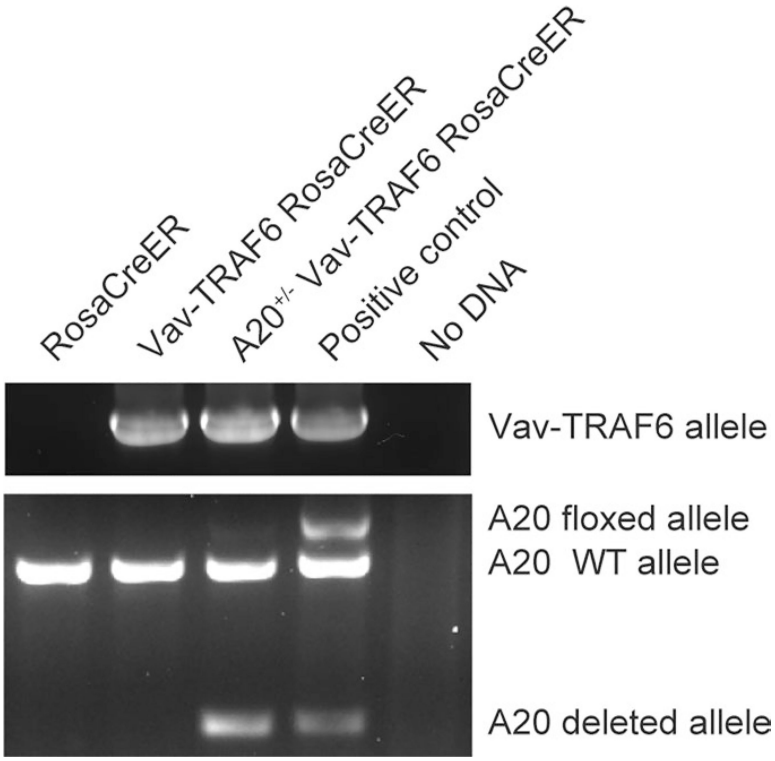

Extended Data Fig. 7 |. Generation of Vav-TRAF6 and A20-deficient mice.
Genotyping analysis of Vav-TRAF6 RosaCreER and $A20^{-/-}$ Vav-TRAF6 RosaCreER mice. A20 floxed allele recombination is shown after Tamoxifen treatment.

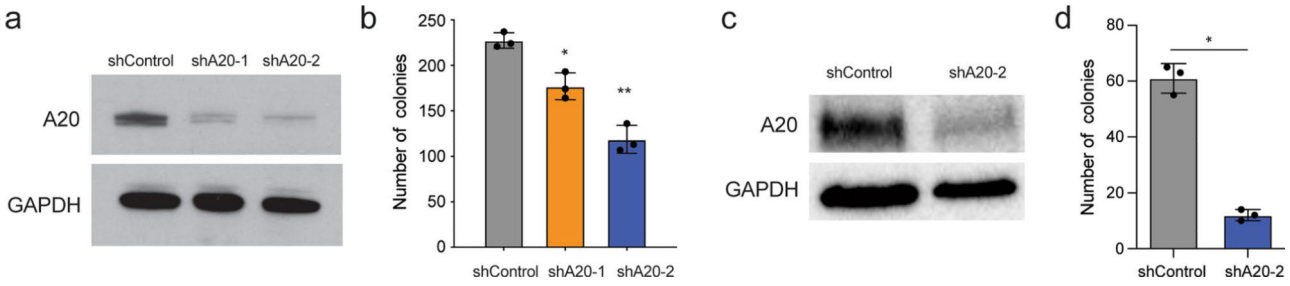

Extended Data Fig. 8 |. A20 knockdown impairs MDSL and THP1 cell function.

a, Immunoblotting of MDSL cells expressing independent shRNAs targeting A20 (shA20) or non-targeting shRNA (shControl). Shown is an immunoblot from a single biological replicate. **b**, Colony forming potential of MDSL cells expressing shRNAs targeting A20 (shA20) or non-targeting shRNA (shControl) in methylcellulose. Results are presented as mean ±s.e.m., for n = 3 independent biological replicates, * P = 0.006, ** P = 0.0004. **c**, Immunoblotting of THP1 cells expressing an shRNA targeting A20 (shA20) or non-targeting shRNA (shControl). Shown is an immunoblot from a single biological replicate. **d**, Colony forming potential of THP1 cells expressing shRNAs targeting A20 or non-targeting shRNA (shControl) in methylcellulose. Results are presented as mean± s.e.m., for $n = 3$ independent biological replicates. *, P = 0.0001. Statistical analysis in **b,d** was performed by a two-tailed Student's *t*-test.

Supplementary Material

Refer to Web version on PubMed Central for supplementary material.

Acknowledgements

This work was supported in parts by the National Institutes of Health (grant nos. R35HL135787, R01DK102759, R01DK113639 to D.T.S.), Cancer Free Kids (D.T.S.), Cincinnati Childrens Hospital Research Foundation (D.T.S.), The Uehara Memorial Foundation (T.M.), The Waksman Foundation of Japan (T.M.), The Mochida Memorial Foundation for Medical and Pharmaceutical Research (T.M.), Japan Society for the Promotion of Science (T.M.) and Ohio State University Comprehensive Cancer Center (T.M.). T.M. is a Leukemia and Lymphoma Society Special Fellow. D.T.S. is a Leukemia and Lymphoma Society Scholar. We thank J. Bailey and V. Summey for assistance with transplantations (Comprehensive Mouse and Cancer Core at CCHMC), and M.-D. Filippi, D. Lucas, D. Reynaud and the Starczynowski laboratory for insightful suggestions and feedback.

References

1. Nimer SD Myelodysplastic syndromes. Blood 111, 4841–4851 (2008). [PubMed: 18467609]
2. Nilsson L et al. Involvement and functional impairment of the $CD34^{+}CD38^{-}Thy\text{-}1^{+}$ hematopoietic stem cell pool in myelodysplastic syndromes with trisomy 8. Blood 100, 259–267 (2002). [PubMed: 12070035]
3. Nilsson L et al. Isolation and characterization of hematopoietic progenitor/ stem cells in 5q-deleted myelodysplastic syndromes: evidence for involvement at the hematopoietic stem cell level. Blood. 96, 2012–2021 (2000). [PubMed: 10979941]
4. Muto T et al. Concurrent loss of *Ezh2* and *Tet2* cooperates in the pathogenesis of myelodysplastic disorders. J. Exp. Med. 210, 2627–2639 (2013). [PubMed: 24218139]
5. Fang J et al. Ubiquitination of hnRNPA1 by TRAF6 links chronic innate immune signaling with myelodysplasia. Nat. Immunol. 18, 236–245 (2017). [PubMed: 28024152]

6. Thanopoulou E et al. Engraftment of NOD/SCID-μ2 microglobulin null mice with multilineage neoplastic cells from patients with myelodysplastic syndrome. Blood 103, 4285–4293 (2004). [PubMed: 14962905]
7. Oishi Y & Manabe I Macrophages in age-related chronic inflammatory diseases. NPJ Aging Mech. Disease 2, 16018 (2016).
8. Pietras EM Inflammation: a key regulator of hematopoietic stem cell fate in health and disease. Blood 130, 1693–1698 (2017). [PubMed: 28874349]
9. Barreyro L, Chlon TM & Starczynowski DT Chronic immune response dysregulation in MDS pathogenesis. Blood 132, 1553–1560 (2018). [PubMed: 30104218]
10. Varney ME et al. Loss of *Tifab*, a del(5q) MDS gene, alters hematopoiesis through derepression of Toll-like receptor-TRAF6 signaling. J. Exp. Med. 212, 1967–1985 (2015). [PubMed: 26458771]
11. Starczynowski DT et al. Identification of miR-145 and miR-146a as mediators of the 5q- syndrome phenotype. Nat. Med. 16, 49–58 (2010). [PubMed: 19898489]
12. Starczynowski DT et al. Genome-wide identification of human microRNAs located in leukemia-associated genomic alterations. Blood 117, 595–607 (2011). [PubMed: 20962326]
13. Rhyasen GW et al. Targeting IRAKI as a therapeutic approach for myelodysplastic syndrome. Cancer Cell 24, 90–104 (2013). [PubMed: 23845443]
14. Fang J et al. TRAF6 mediates basal activation of NF-kB necessary for hematopoietic stem cell homeostasis. Cell Rep. 22, 1250–1262 (2018). [PubMed: 29386112]
15. Varney ME et al. Epistasis between TIFAB and miR-146a: neighboring genes in del(5q) myelodysplastic syndrome. Leukemia 31, 491–495 (2017). [PubMed: 27733775]
16. Sato S et al. Toll/IL-1 receptor domain-containing adaptor inducing IFN-β (TRIF) associates with TNF receptor-associated factor 6 and TANK-binding kinase 1, and activates two distinct transcription factors, NF-kB and IFN-regulatory factor-3, in the Toll-like receptor signaling. J. Immunol. 171, 4304–4310 (2003). [PubMed: 14530355]
17. Gohda J, Matsumura T & Inoue J Cutting edge: TNFR-associated factor (TRAF) 6 is essential for MyD88-dependent pathway but not Toll/IL-1 receptor domain-containing adaptor-inducing IFN-β (TRIF)-dependent pathway in TLR signaling. J Immunol. 173, 2913–2917 (2004). [PubMed: 15322147]
18. Schuettpelz LG & Link DC Regulation of hematopoietic stem cell activity by inflammation. Front. Immunol. 4, 204 (2013). [PubMed: 23882270]
19. Zhao JL et al. NF-kB dysregulation in microRNA-146a-deficient mice drives the development of myeloid malignancies. Proc. Natl Acad. Sci. USA 108,9184–9189 (2011). [PubMed: 21576471]
20. Takizawa H et al. Pathogen-Induced TLR4-TRIF Innate Immune Signaling in Hematopoietic Stem Cells Promotes Proliferation but Reduces Competitive Fitness. Cell Stem Cell 21, 225–240.e5 (2017). [PubMed: 28736216]
21. Zhang H et al. Sepsis induces hematopoietic stem cell exhaustion and myelosuppression through distinct contributions of TRIF and MYD88. Stem Cell Rep. 6, 940–956 (2016).
22. Esplin BL et al. Chronic exposure to a TLR ligand injures hematopoietic stem cells. J. Immunol. 186, 5367–5375 (2011). [PubMed: 21441445]
23. Liu A et al. Cutting edge: hematopoietic stem cell expansion and common lymphoid progenitor depletion require hematopoietic-derived, cell-autonomous TLR4 in a model of chronic endotoxin. J. Immunol. 195, 2524–2528 (2015). [PubMed: 26276875]
24. Chavakis T, Mitroulis I & Hajishengallis G Hematopoietic progenitor cells as integrative hubs for adaptation to and fine-tuning of inflammation. Nat. Immunol. 20, 802–811 (2019). [PubMed: 31213716]
25. Waterstrat A, Liang Y, Swiderski CF, Shelton BJ & Van Zant G Congenic interval of CD45/Ly-5 congenic mice contains multiple genes that may influence hematopoietic stem cell engraftment. Blood 115, 408–417 (2010). [PubMed: 19901263]
26. Fang J et al. Myeloid malignancies with chromosome 5q deletions acquire a dependency on an intrachromosomal NF-kB gene network. Cell Rep. 8, 1328–1338 (2014). [PubMed: 25199827]
27. Sanz C, Richard C, Prosper F & Fernandez-Luna JL Nuclear factor k B is activated in myelodysplastic bone marrow cells. Haematologica 87, 1005–1006 (2002). [PubMed: 12217815]

28. Wei Y et al. Global H3K4me3 genome mapping reveals alterations of innate immunity signaling and overexpression of JMJD3 in human myelodysplastic syndrome CD34+ cells. Leukemia 27, 2177–2186 (2013). [PubMed: 23538751]
29. Magness ST et al. In vivo pattern of lipopolysaccharide and anti-CD3-induced NF-kB activation using a novel gene-targeted enhanced GFP reporter gene mouse. J. Immunol. 173, 1561–1570 (2004). [PubMed: 15265883]
30. Sun SC The non-canonical NF-kB pathway in immunity and inflammation. Nat. Rev. Immunol. 17, 545–558 (2017). [PubMed: 28580957]
31. Yamaguchi N, Oyama M, Kozuka-Hata H & Inoue J Involvement of A20 in the molecular switch that activates the non-canonical NF-kB pathway. Sci. Rep. 3, 2568 (2013). [PubMed: 24008839]
32. Wertz IE et al. De-ubiquitination and ubiquitin ligase domains of A20 downregulate NF-kB signalling. Nature 430, 694–699 (2004). [PubMed: 15258597]
33. Lee EG et al. Failure to regulate TNF-induced NF-kB and cell death responses in A20-deficient mice. Science 289, 2350–2354 (2000). [PubMed: 11009421]
34. Bird L TET2: the terminator. Nat. Rev. Immunol. 15, 598 (2015).
35. Zhang Q et al. Tet2 is required to resolve inflammation by recruiting Hdac2 to specifically repress IL-6. Nature. 525, 389–393 (2015). [PubMed: 26287468]
36. Cai Z et al. Inhibition of inflammatory signaling in *Tet2* mutant preleukemic cells mitigates stress-induced abnormalities and clonal hematopoiesis. Cell Stem Cell 23, 833–849 (2018). [PubMed: 30526882]
37. Rhyasen GW et al. An MDS xenograft model utilizing a patient-derived cell line. Leukemia 28, 1142–1145 (2014). [PubMed: 24326684]
38. Kumar MS et al. Coordinate loss of a microRNA and protein-coding gene cooperate in the pathogenesis of 5q-syndrome. Blood 118, 4666–4673 (2011). [PubMed: 21873545]
39. Nakagawa MM, Thummar K, Mandelbaum J, Pasqualucci L 8c Rathinam, C. V. Lack of the ubiquitin-editing enzyme A20 results in loss of hematopoietic stem cell quiescence. J. Exp. Med. 212, 203–216 (2015). [PubMed: 25624445]
40. Cull AH, Snetsinger B, Buckstein R, Wells RA 8c Rauh, M. J. Tet2 restrains inflammatory gene expression in macrophages. Exp. Hematol. 55, 56–70.e13 (2017). [PubMed: 28826859]
41. Ma S et al. Epigenetic regulator CXXC5 recruits DNA demethylase Tet2 to regulate TLR7/9-elicited IFN response in pDCs. J. Exp. Med. 214, 1471–1491 (2017). [PubMed: 28416650]
42. Leoni C et al. Dnmt3a restrains mast cell inflammatory responses. Proc. Natl Acad. Sci. USA 114, E1490–E1499 (2017). [PubMed: 28167789]
43. Li X et al. Methyltransferase Dnmt3a upregulates HDAC9 to deacetylate the kinase TBK1 for activation of antiviral innate immunity. Nat. Immunol. 17, 806–815 (2016). [PubMed: 27240213]
44. Lee SC et al. Synthetic lethal and convergent biological effects of cancer-associated spliceosomal gene mutations. Cancer Cell 34, 225–241.e8 (2018). [PubMed: 30107174]
45. Smith MA et al. U2AF1 mutations induce oncogenic IRAK4 isoforms and activate innate immune pathways in myeloid malignancies. Nat. Cell Biol. 21, 640–650 (2019). [PubMed: 31011167]
46. Pollyea DA et al. Myelodysplastic syndrome-associated spliceosome gene mutations enhance innate immune signaling. Haematologica 104, e388–e392 (2019). [PubMed: 30846499]
47. Ulas T et al. S1OO-alarmin-induced innate immune programming protects newborn infants from sepsis. Nat. Immunol. 18, 622–632 (2017). [PubMed: 28459433]
48. Shi H et al. Chemokine (C-X-C motif) ligand 1 and CXCL2 produced by tumor promote the generation of monocytic myeloid-derived suppressor cells. Cancer Sci. 109, 3826–3839 (2018). [PubMed: 30259595]
49. Tavares RM et al. The ubiquitin modifying enzyme A20 restricts B cell survival and prevents autoimmunity. Immunity 33, 181–191 (2010). [PubMed: 20705491]
50. Fang J et al. A calcium- and calpain-dependent pathway determines the response to lenalidomide in myelodysplastic syndromes. Nat Med. 22, 727–734 (2016). [PubMed: 27294874]
51. Haeussler M et al. Evaluation of off-target and on-target scoring algorithms and integration into the guide RNA selection tool CRISPOR. Genome Biol. 17, 148 (2016). [PubMed: 27380939]

52. Choi K & Ratner N iGEAK: an interactive gene expression analysis kit for seamless workflow using the R/shiny platform. BMC Genomics 20, 177 (2019). [PubMed: 30841853]

53. Pellagatti A et al. Deregulated gene expression pathways in myelodysplastic syndrome hematopoietic stem cells. Leukemia 24, 756–764 (2010). [PubMed: 20220779]

54. Gerstung M et al. Combining gene mutation with gene expression data improves outcome prediction in myelodysplastic syndromes. Nat. Commun. 6, 5901 (2015). [PubMed: 25574665]

55. Subramanian A et al. Gene set enrichment analysis: a knowledge-based approach for interpreting genome-wide expression profiles. Proc. Natl Acad. Sci. USA 102, 15545–15550 (2005). [PubMed: 16199517]

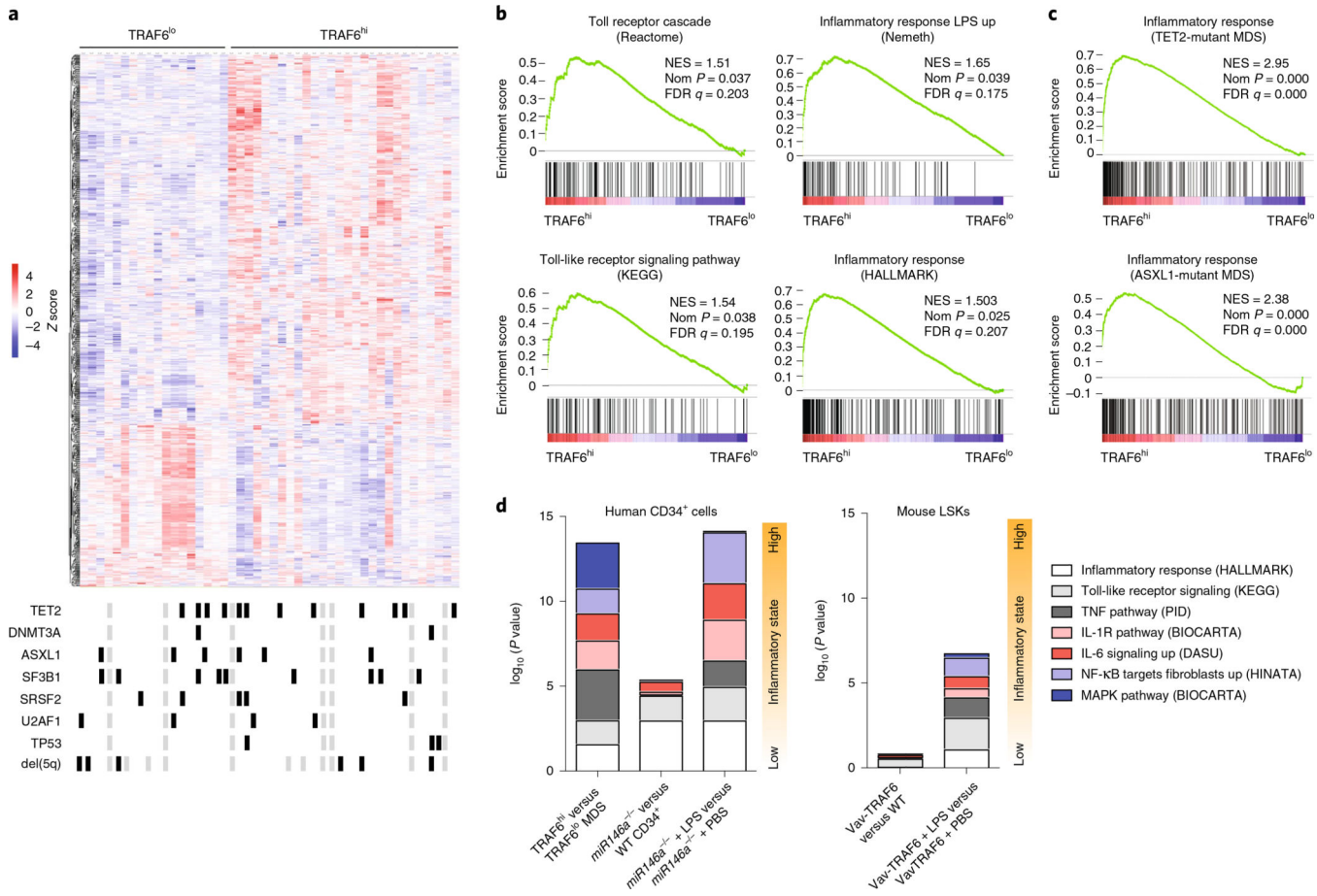

Fig. 1 |. MDS HSPC are associated with inflammatory states.

a, Heatmap of all differentially expressed genes in CD34+ MDS BM cells (GSE58831,1.5-fold, P<0.05), stratified based on high (n = 28, Z=> 1.0) and low (n = 18, Z<-1.0) TRAF6 expression. Each row represents individual genes arranged by semiunsupervised clustering analysis based on the Z score (see Supplementary Table 1). Columns represent individual MDS patients. Reoccurring somatic mutations and cytogenetic alterations in the MDS patient samples are shown by black bars at the bottom. Gray bars indicate no available data. **b**, GSEA gene signatures from 'TRAF6 high' (TRAF6^{hi}) CD34+ MDS cells as compared to 'TRAF6 low' (TRAF6^{10}) CD34^{+} MDS cells. **c**, GSEA gene signatures from TET2 or ASXL1 mutant CD34^{+}TRAF6^{hi} MDS cells as compared to CD34+TRAF6^{10} MDS cells. **d**, RNA sequencing of human *miR146a*$^{-/-}$ and WT CD34+ BM cells or Vav-TRAF6 and WT LSK BM cells were stimulated in vitro for 90 min with 1 γg ml^{-1} of LPS (or PBS) (see Supplementary Tables 2–8). Results are presented as mean ±s.e.m., for n = 3 independently treated samples. The inflammatory state for each group was determined using the GSEA profiles established from CD34^{+}TRAF6^{hi} MDS cells. The indicated inflammatory gene signatures are arranged by P value ($\log_{10}$).

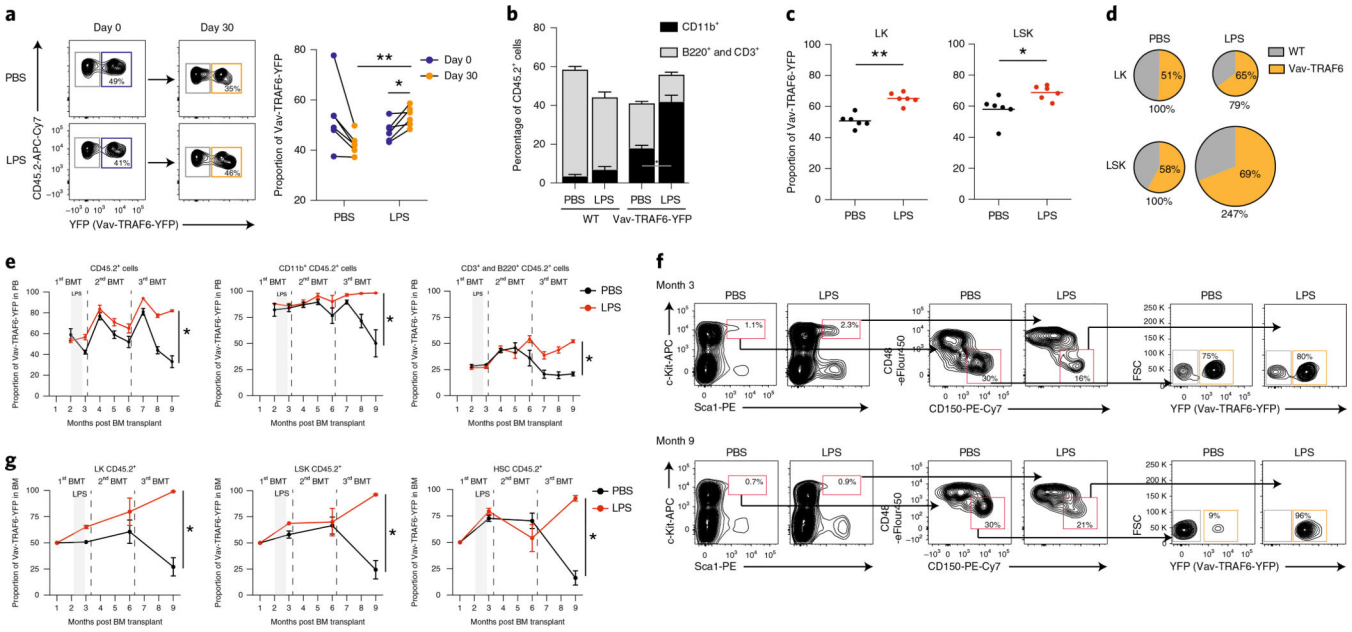

Fig. 2 |. TLR-TRAF6-primed HSPCs outcompete WT HSPCs with LD-LPS.

a, Left panel, representative flow cytometric profiles of YFP$^+$ (Vav-TRAF6-YFP) cells in the PB of chimeric mice before and after LPS or vehicle (PBS) treatment. Right panel, the proportion of YFP$^+$ (Vav-TRAF6-YFP) cells relative to YFP$^-$ (WT) cells before and after LPS or vehicle (PBS) treatment. Data represent the mean±s.e.m., $n = 6$ mice per group (*P< 0.05, **P< 0.0001). **b**, The proportion of myeloid (CD11b$^+$) and lymphoid (CD3$^+$ and B220$^+$) YFP$^-$ (WT) and YFP$^+$ (Vav-TRAF6-YFP) cells in the PB after LPS or vehicle (PBS) treatment. Data represent the mean±s.e.m., $n = 6$ mice per group. (*P< 0.05). **c**, The proportion of YFP$^+$ (Vav-TRAF6-YFP) cells in LK and LSK populations 30 days after treatment with LPS or vehicle (PBS). Data represent the mean±s.e.m., $n = 6$ mice per group (*P< 0.05, **P< 0.01). **d**, Pie charts indicating the relative and absolute frequency of each population (LK and LSK) in the mice treated with LD-LPS as compared to the mice treated with PBS. Data represent the mean, $n = 6$ mice per group. **e**, Chimerism of YFP$^+$ (Vav-TRAF6-YFP) cells in all CD45.2$^+$ (left panel), myeloid (CD11b$^+$, middle panel) and lymphoid (B220$^+$ and CD3$^+$, right panel) in the PB at the indicated time points. Gray bar indicates in vivo LD-LPS treatment. Data represent the mean±s.e.m., $n = 5$ mice per group (*P = 0.05). **f**, Representative flow cytometric profiles of YFP$^+$ (Vav-TRAF6-YFP) cells in HSC at 12 weeks after primary (upper panel) and tertiary transplantation (lower panel). **g**, Chimerism of YFP$^+$ (Vav-TRAF6-YFP) cells in LK, LSK and HSC in the BM at the indicated time points. Gray bar indicates in vivo LPS treatment. Data represent the mean ±s.e.m., $n = 5$ mice per group (*P< 0.05). Statistical analysis in **a,c,e,g** was performed by a two-tailed Student's t-test.

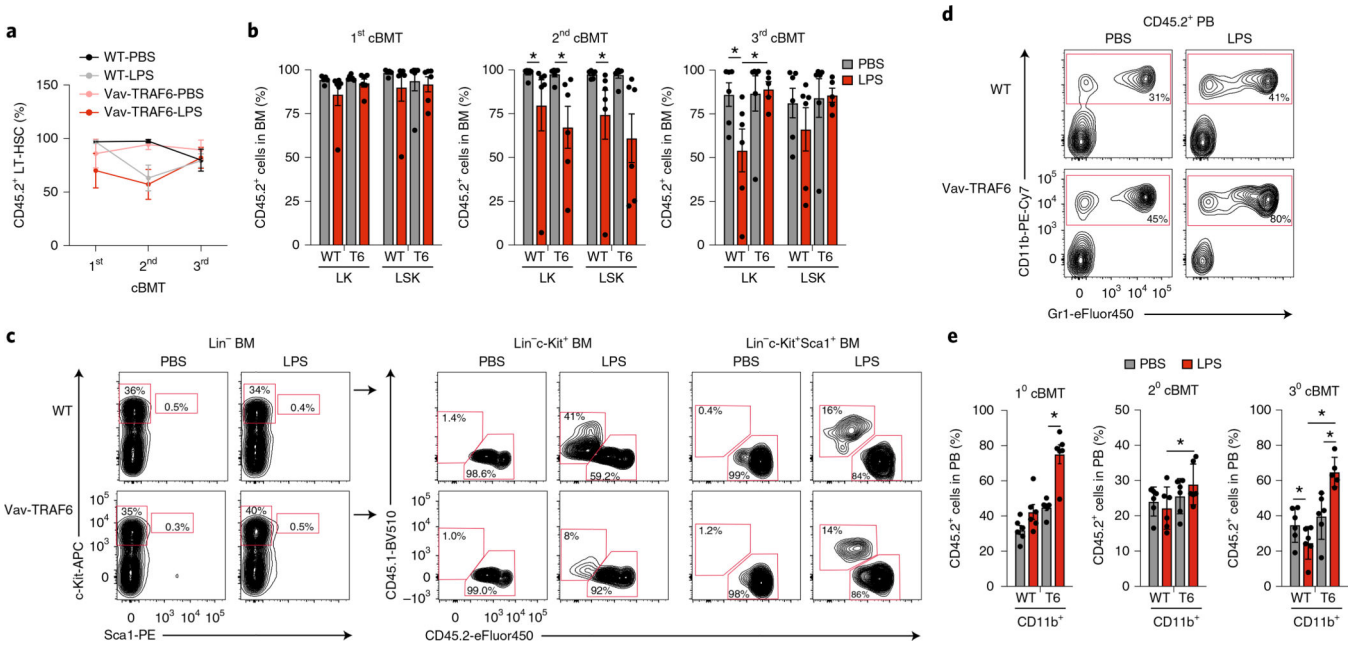

Fig. 3 |. Overexpression of TRAF6 alters the response of hematopoietic cells to LD-LPS.

a, Proportion of donor-derived CD45.2$^+$ cells in HSC cells after primary, secondary and tertiary transplantation. Error bars indicate s.e.m. for $n = 5$ mice per group. **b**, Proportion of donor-derived CD45.2$^+$ cells in LK and LSK cells after primary, secondary and tertiary transplantation. Data represent the mean ± s.e.m., $n = 5$ mice per group (*$P < 0.05$). **c**, Representative flow cytometric analysis of CD45.2 proportions in LK and LSK cells at 12 weeks after tertiary transplantation. **d**, Representative flow cytometric profiles of CD11b+ myeloid cells in CD45.2$^+$ PB at 4weeks post transplantation. **e**, Proportion of myeloid (CD11b$^+$) cells in the donor-derived compartment (gated on CD45.2$^+$) after primary, secondary and tertiary transplantation. Data represent the mean ± s.e.m., $n = 5$ mice per group (*$P < 0.05$). Statistical analysis in **b,e** was performed by a one-tailed Student's *t*-test.

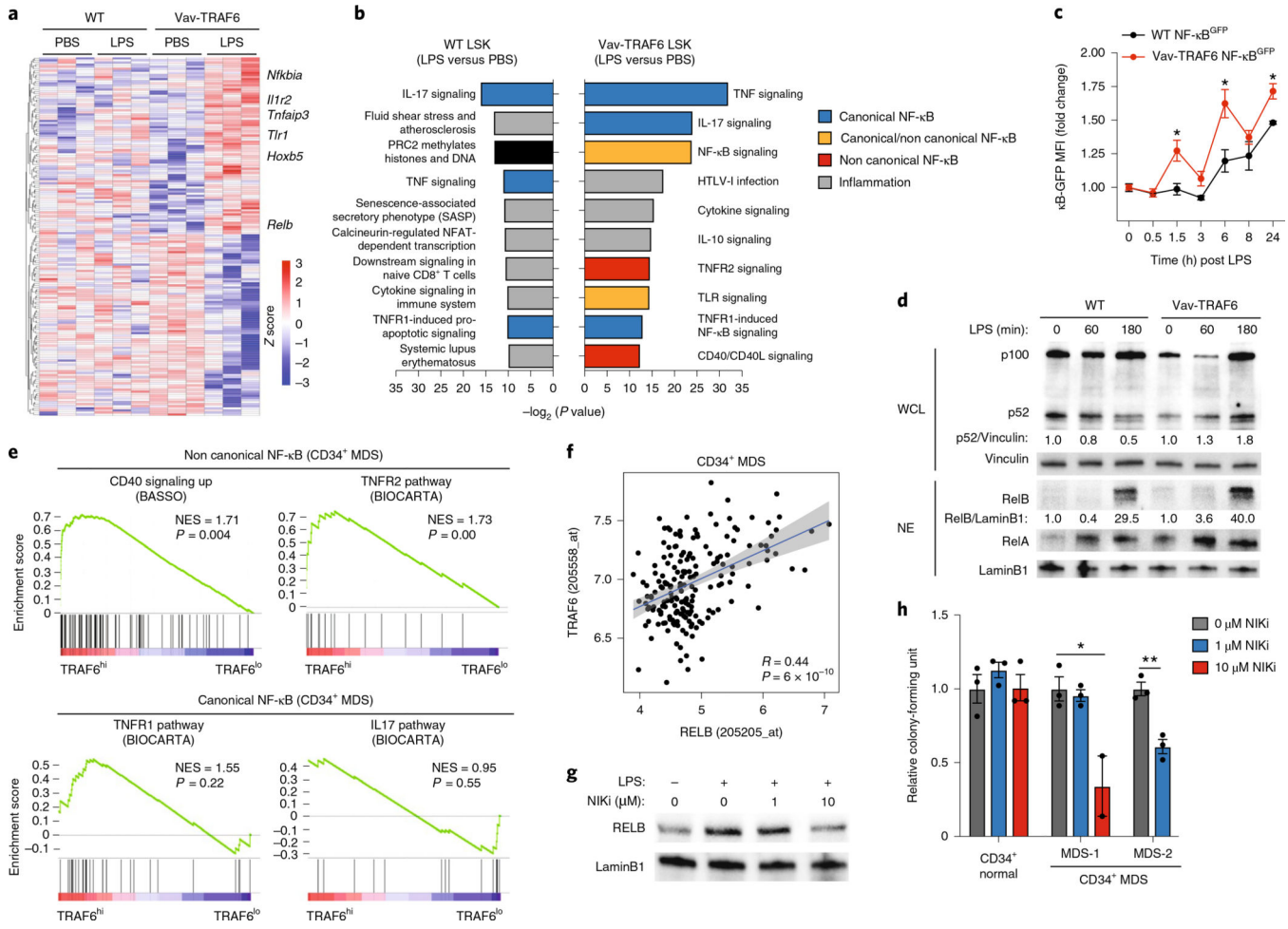

Fig. 4 |. LD-LPS stimulation of TLR-TRAF6-primed HSPC results in noncanonical NF-kB signaling.

a, Heatmap of differentially expressed genes in WT or Vav-TRAF6 LSK cells treated with LPS or PBS (1.5-fold, $P< 0.05$, $n = 3$ per group). **b**, TOPP gene analysis of the top ten enriched pathways in WT and Vav-TRAF6 LSK cells treated with LPS as compared to WT or Vav-TRAF6 control, respectively. **c**, Mean fluorescence intensity (MFI) of GFP in Lin^- BM cells from WT (WT-NF-kB-GFP) and Vav-TRAF6 (Vav-TRAF6-NF-kB-GFP) NF-kB-GFP reporter mice treated in vitro with LPS (1 μgml^{-1}). Results are presented as mean ±s.e.m., for $n = 3$ independently treated samples (*$P< 0.05$). **d**, Immunoblotting of c-Kit^+ BM whole cell lysates (WCL) and nuclear extracts (NEs) isolated from WT or Vav-TRAF6 mice after treatment with LPS (1 μgml^{-1}). Shown is a representative blot from two independent replicates. **e**, GSEA plots for noncanonical NF-kB (upper panel) and canonical NF-kB (lower panel) pathways in $CD34^+TRAF6^{hi}$ MDS BM cells as compared to CD34+$TRAF6^{10}$ MDS BM cells. **f**, Regression analysis between RELB and TRAF6 mRNA expression in $CD34^+$ MDS BM cells ($R = 0.44$; $P=6\times10^{-10}$). **g**, Immunoblotting of nuclear extracts from THP1 cells treated with LPS (100 ng ml^{-1}) and/or NIK inhibitor (NIKi). Shown is a representative blot from two independent replicates. **h**, $CD34^+$ del(5q) MDS BM and normal $CD34^+$ BM cells treated with NIKi were evaluated for colony formation in methylcellulose. Results are presented as mean±s.e.m., for $n = 3$ independent technical

replicates(*P<0.05, **P< 0.01). Statistical analysis in **c,h** was performed by a two-tailed Student's *t*-test.

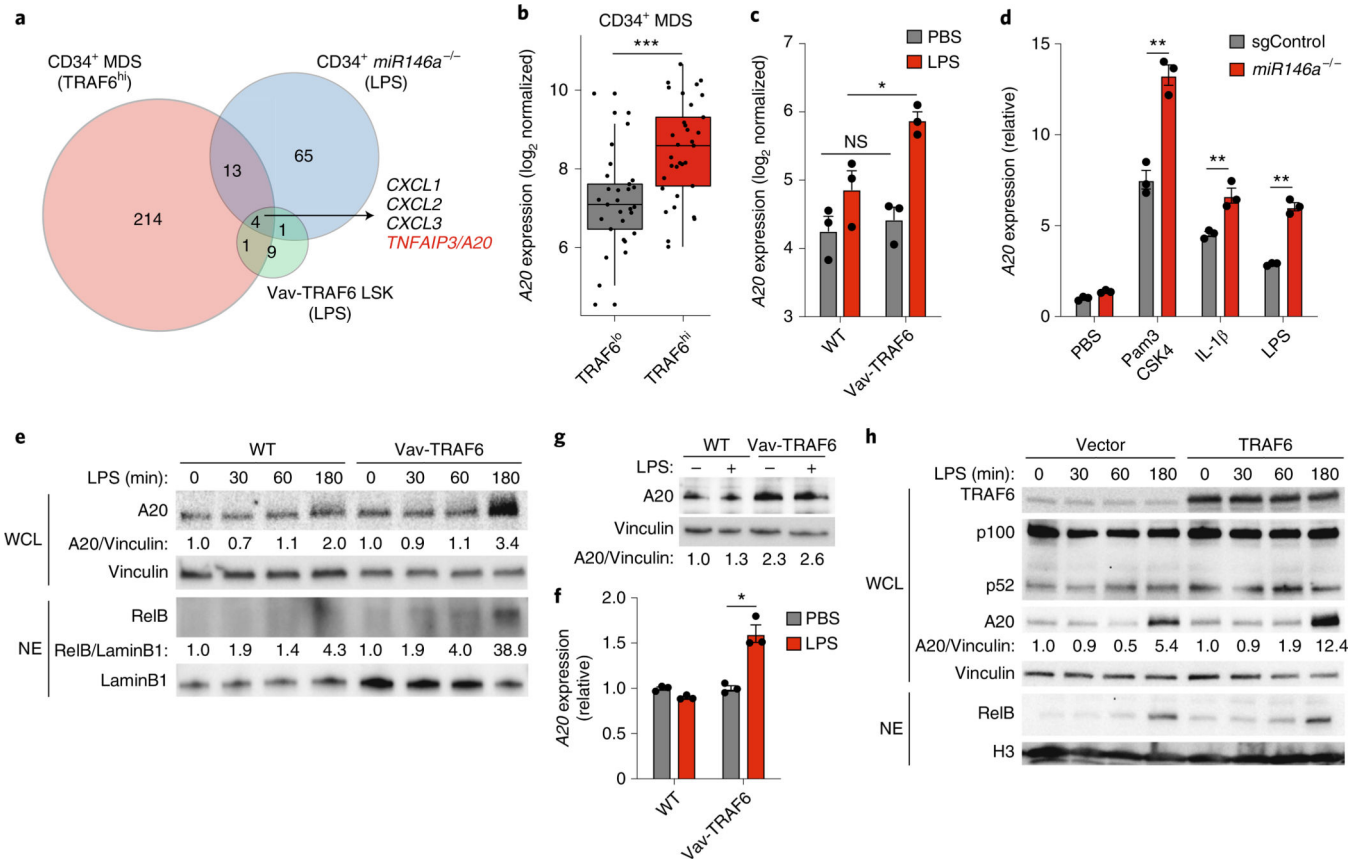

Fig. 5 |. Noncanonical NF-kB activation correlates with A20 expression in TLR-TRAF6 primed HSPCs.

a, Venn diagram of upregulated genes (1.5-fold, P<0.0.5) in CD34^{+}TRAF6^{hi} MDS BM cells (relative to CD34^{+}TRAF6^{10} MDS BM), LPS-stimulated *miR146a*$^{-/-}$ human CD34^{+} BM (relative to *miR146a*$^{-/-}$ human CD34^{+} BM treated with PBS and normal CD34^{+} BM±LPS) and LPS-stimulated Vav-TRAF6 LSK cells (relative to Vav-TRAF6 LSK treated with PBS and WT LSK±LPS). **b**, A20 mRNA expression in TRAF6^{hi} and TRAF6^{10} CD34^{+} MDS BM cells (GSE19429) (***P<0.001). **c**, A20 mRNA expression in WT and Vav-TRAF6 LSK cells treated with either PBS or LPS (1μgml^{-1}) for 90 min, as determined by RNA sequencing. Results are presented as mean±s.e.m., for n = 3 independently treated samples (*P< 0.05). **d**, A20 mRNA expression in WT and *miR146a*$^{-/-}$ human CD34^{+} BM cells treated with PBS, Pam3CSK4 (1μgml^{-1}), IL-1β (10 ngml^{-1}) or LPS (1μgml^{-1}) for 90 min. Results are presented as mean±s.e.m., for n = 3 independent biological replicates (**P<0.01). **e**, Immunoblot analysis of A20 and Relb in whole cell lysates (WCL) and nuclear extracts (NEs) from WT and Vav-TRAF6 c-Kit^{+} BM cells after LPS treatment (1μgml^{-1}). **f**, A20 mRNA expression in c-Kit^{+} BM cells from WT and Vav-TRAF6 mice treated with LD-LPS (1μg g^{-1}) or vehicle for 16 h. Error bars indicate s.e.m. for n = 3 technical replicates from individual mice (*P<0.05). **g**, Immunoblot analysis of WT and Vav-TRAF6 c-Kit^{+} BM cells from WT and Vav-TRAF6 mice treated with LD-LPS (1μg g^{-1}) or vehicle twice a week for 30 days. Shown below is the relative expression of the indicated proteins. The immunoblot is from three pooled mice per group performed as a single replicate. **h**, Immunoblotting of THP1 cells expressing TRAF6 or empty vector

treated with LPS (100 ng ml^{-1}). Shown is a representative blot from two independent replicates. Statistical analysis in **b-d,f** was performed by a two-tailed Student's *t*-test. NS, nonsignificant.

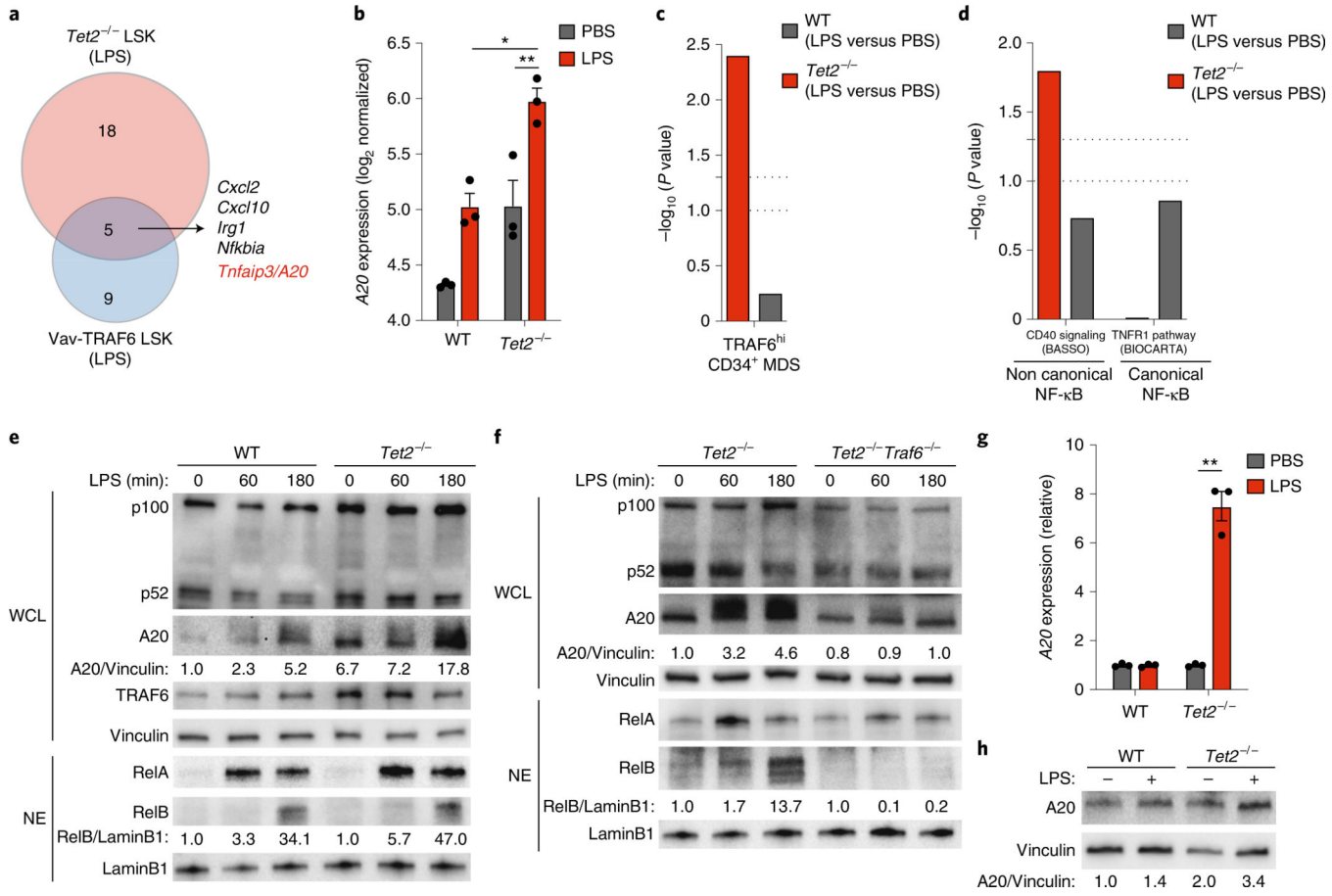

Fig. 6 |. A20 expression and noncanonical NF-kB activation occurs in TET2-deficient HSPC.

a, Venn diagram of upregulated genes (1.5-fold, $P< 0.0.5$) in LPS-stimulated *Tet2*$^{-/-}$ LSK (relative to *Tet2*$^{-/-}$ LSK with PBS and *Tet2*$^{fl/fl}$ LSK±LPS), and LPS-stimulated Vav-TRAF6 LSK cells (relative to Vav-TRAF6 LSK treated with PBS and WT LSK ± LPS). **b**, A20 mRNA expression in Tet2$^{fl/fl}$ and Tet2$^{fl/fl}$VavCre LSK cells treated with either PBS or LPS (1 μgml^{-1}) for 90 min was determined by RNA sequencing. Results are presented as mean ±s.e.m., for $n = 3$ independently treated samples (*$P< 0.05$, **$P<0.01$). **c**, Enrichment analysis of upregulated genes from CD34^{+}TRAF6^{hi} MDS BM cells in *Tet2*$^{fl/fl}$ LSK (WT) or *Tet2*$^{fl/fl}$ VavCre LSK (*Tet2*$^{-/-}$) treated with LPS (1.5-fold, $P< 0.05$). **d**, Enrichment analysis of upregulated genes from canonical (CD40 signaling, NES = 1.56, $P = 0.02$) and noncanonical (TNFR pathway) NF-kB signaling in *Tet2*$^{fl/fl}$ LSK (WT) or *Tet2*$^{fl/fl}$ VavCre LSK (*Tet2*$^{-/-}$) treated with LPS (1.5-fold. $P<0.05$). **e**, Immunoblotting of c-Kit^{+} BM cells isolated from *Tet2*$^{fl/fl}$ (WT) or *Tet2*$^{fl/fl}$ VavCre (*Tet2*$^{-/-}$) mice stimulated with LPS (1 μgml^{-1}). Shown is a representative blot from two independent replicates. Below is the relative expression of the indicated proteins. **f**, Immunoblotting of c-Kit^{+} BM cells isolated from *Tet2*$^{fl/fl}$*Traf6*$^{fl/fl}$ VavCre (*Tet2*$^{-/-}$*Traf6*$^{-/-}$) or *Tet2*$^{fl/fl}$ VavCre (*Tet2*$^{-/-}$) mice stimulated with LPS (1 μgml^{-1}). Below is the relative expression of the indicated proteins. **g**, A20 mRNA expression in *Tet2*$^{fl/fl}$ or *Tet2*$^{fl/fl}$VavCre (*Tet2*) c-Kit^{+} BM cells after 16 h of in vivo LPS (1 μg g^{-1}) treatment. Results are presented as mean±s.e.m., for $n = 3$ independent replicates, **$P< 0.001$. **h**, Immunoblot analysis of A20 in *Tet2*$^{fl/fl}$ and *Tet2*$^{fl/fl}$VavCre c-kit^{+} BM cells

after 30 days of in vivo LPS (1 μg g^{-1}) treatment. The immunoblot is from three pooled mice per group performed as a single replicate. Below is the relative expression of the indicated proteins. Statistical analysis in **b** was performed by a one-tailed Student's *t*-test. Statistical analysis in **g** was performed by a two-tailed Student's *t*-test.

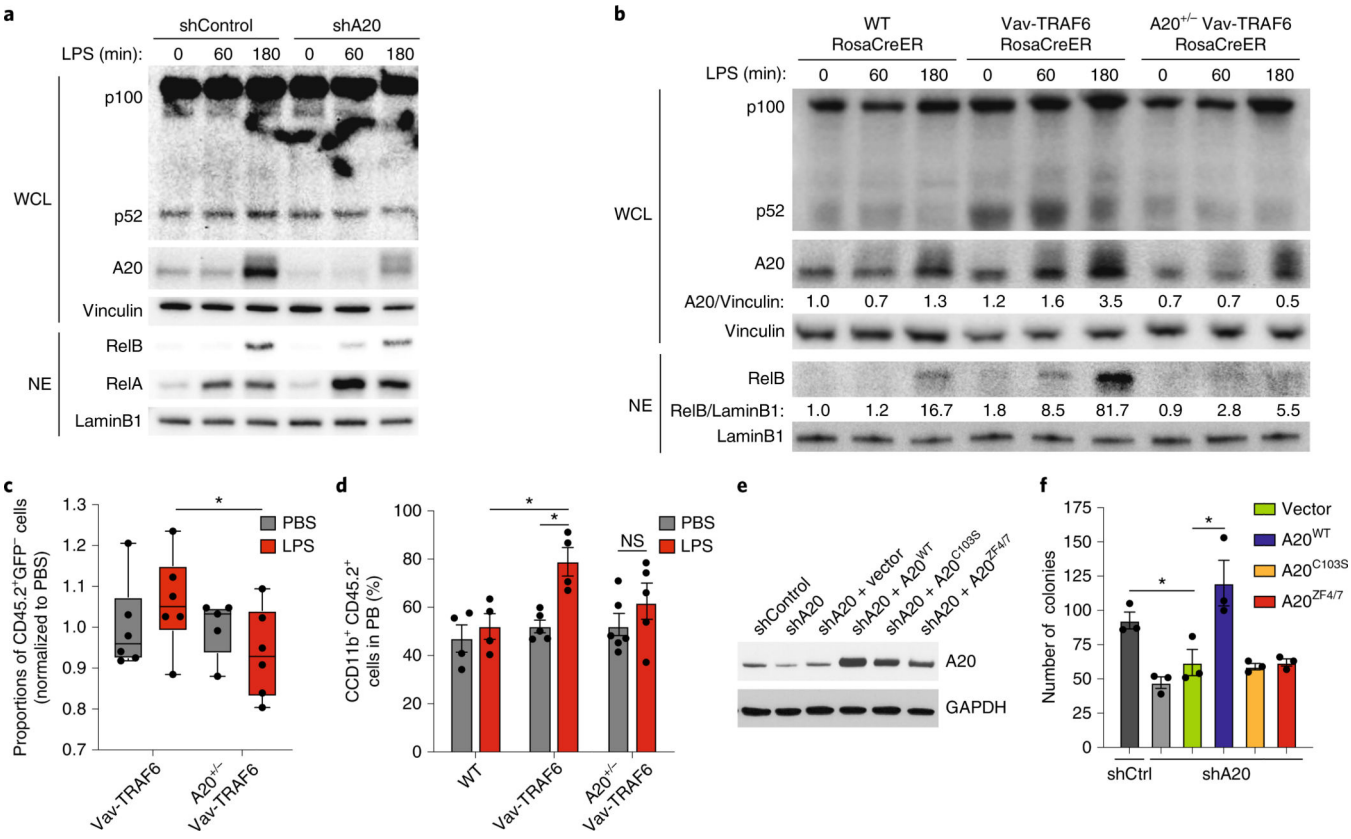

Fig. 7 |. Deletion of A20 prevents noncanonical NF-kB signaling and rescues the competitive advantage of TLR-TRAF6-primed HSPCs during LD-LPS.

a, Immunoblotting of THP1 cells expressing shA20 or non-targeting shRNA (shControl) treated with LPS (100 ng ml^{-1}). Shown is a representative blot from two independent replicates. **b**, Immunoblotting of c-Kit^+ BM isolated from WT, Vav-TRAF6 RosaCreER and $A20^{+/-}$ Vav-TRAF6 RosaCreER mice treated with LPS (1 μgml^{-1}). Shown is a representative blot from two independent replicates. Below is the relative expression of the indicated proteins. **c**, The proportion of PB GFP^- cells in chimeric mice with Vav-TRAF6 RosaCreER or $A20^{+/-}$ Vav-TRAF6 RosaCreER BM cells and WT CD45.2 BM cells (expressing a UBC-GFP transgene, hereafter WT-GFP) after 4 weeks of twice a week treatment with LD-LPS (1 μg g^{-1}) or vehicle. The data shown are after the last LD-LPS treatment as normalized values to each PBS control. Data represent the mean ± s.e.m., $n = 5$ mice per group, *$P < 0.05$. **d**, Percentage of myeloid ($CD11b^+$) cells in donor-derived CD45.2 PB cells was determined at 4 weeks postcompetitive transplantation of CD45.2 WT, Vav-TRAF6 RosaCreER and $A20^{+/-}$ Vav-TRAF6 RosaCreER BM cells isolated from mice treated with LD-LPS (1 μg g^{-1}) or vehicle twice a week for 4 weeks along with CD45.1 competitor BM cells. Data represent the mean ± s.e.m., $n = 4$ mice per group, *$P < 0.05$. **e**, Immunoblotting of MDSL cells expressing shA20 or non-targeting shRNA (shControl) and cDNAs expressing WT or mutant A20. Shown is an immunoblot from a single biological replicate. **f**, Colony forming potential of MDSL cells expressing shA20 or non-targeting shRNA (shControl) in methylcellulose. Results are presented as mean ±s.d., for $n = 3$ independent samples. *$P < 0.05$. Statistical analysis in **c** was performed by a one-tailed

Student's *t*-test. NS, nonsignificant. Statistical analysis in **d,f** was performed by a two-tailed Student's *t*-test.